

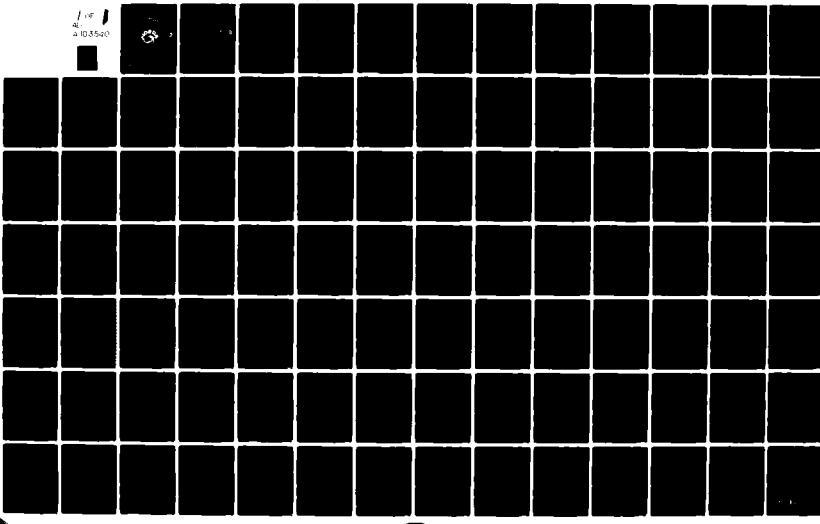
AD-A103 540

NAVAL OCEAN RESEARCH AND DEVELOPMENT ACTIVITY NSTL S-ETC F/8 8/10  
A SUMMARY OF PAPERS RELATED TO MESOSCALE AND LARGE-SCALE OCEAN -ETC(IU)  
JUN 81 M E HURLBURT  
NORDA-TN-109-VOL-1

UNCLASSIFIED

NL

1 of 1  
403540

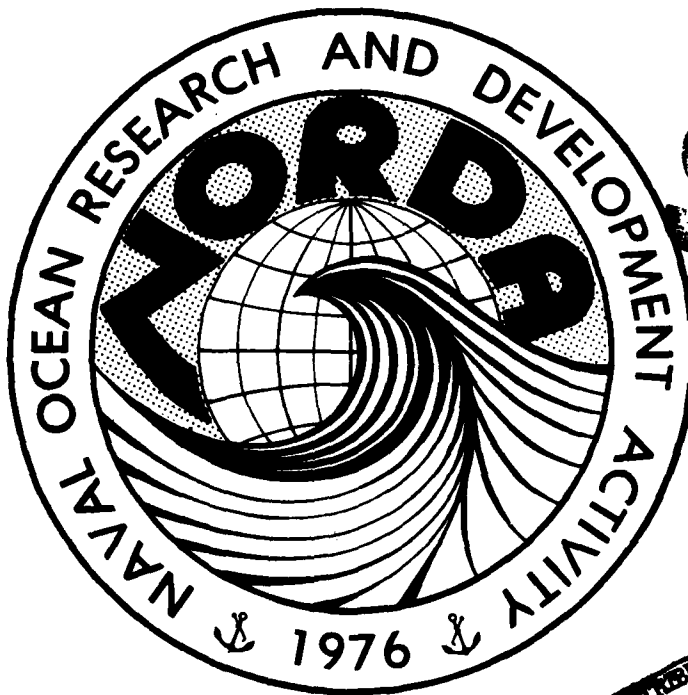


12

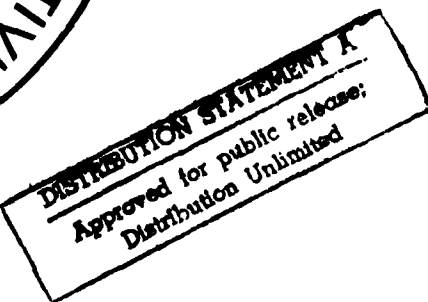
Naval Ocean Research  
and Development Activity  
NSTL Station, Mississippi 39529

A Summary of Papers Related to  
Mesoscale and Large-Scale  
Ocean Modeling, Volume I

ADA103540



DTIC  
SELECTED  
SEP 1 1981



Harley E. Hurlburt

Ocean Science and Technology Laboratory  
Numerical Modeling Division

June 1981

22814

DTIC FILE COPY

819 01 021

NORDA Technical Note 109

A SUMMARY OF PAPERS RELATED TO  
MESOSCALE AND LARGE-SCALE OCEAN MODELING.

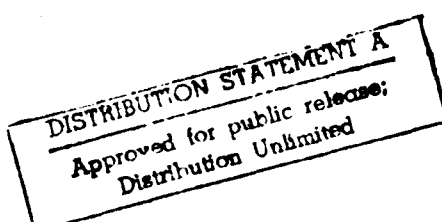
VOLUME I.

HARLEY E. HURLBURT

JUN 1981

DTIC  
SELECTED  
SEP 1 1981  
S D H

ENVIRONMENTAL SIMULATION BRANCH  
CODE 322  
NAVAL OCEAN RESEARCH AND DEVELOPMENT ACTIVITY  
NSTL STATION, MISSISSIPPI 39529



## ABSTRACT

This technical note contains summaries of the important ideas and results from 13 papers related to mesoscale and large scale ocean modeling. Most of the papers represent major contributions to our understanding of the dynamics and energetics of mesoscale eddies and their interaction with ocean currents and with each other. Understanding the nature of flow instabilities associated with the generation and evolution of the eddies is an important aspect of the problem which receives much attention in these papers. Most of the numerical simulations utilized simple two-layer, eddy-resolving, quasi-geostrophic models; a small number used primitive equation models.

5

Accession For	<input checked="" type="checkbox"/>
NTIS Serial	<input type="checkbox"/>
DTIC Title	<input type="checkbox"/>
Unnumbered	<input type="checkbox"/>
Justification	
By	<input type="checkbox"/>
Distribution	<input type="checkbox"/>
Availability Codes	<input type="checkbox"/>
Avail. and/or	<input type="checkbox"/>
Dist Specifi	<input type="checkbox"/>

A

#### ACKNOWLEDGEMENTS

Mrs. Charlene Parker is due many thanks for typing the manuscript. This technical note was completed as part of an objective under the Navy's Merit Pay System. Because of the informal nature of the document, it makes liberal use of quotes and paraphrased statements from the original papers without further indication. It is intended for use by NORDA Code 322 personnel and other interested personnel at NORDA.

## LIST OF PAPERS SUMMARIZED

## Page

1.	Haidvogel, D. B., 1979: A discussion of certain modeling factors which influence the results of eddy-resolving ocean circulation studies. <u>Dyn. Atmos. Oceans</u> , <u>3</u> , 181-190.	1
2.	Robinson, A. R., D. E. Harrison, and D. B. Haidvogel, 1979: Mesoscale eddies and general ocean circulation models. <u>Dyn. Atmos. Oceans</u> , <u>3</u> , 143-180.	5
3.	Holland, W. R., 1975: Energetics of baroclinic oceans. <u>Numerical Models of Ocean Circulation</u> , National Academy of Sciences, Washington, DC, pp. 168-177.	9
4.	Holland, W. R., 1978: The role of mesoscale eddies in the general circulation of the ocean - Numerical experiments using a wind-driven quasi-geostrophic model. <u>J. Phys. Oceanogr.</u> , <u>8</u> , 363-392.	11
5.	McWilliams, J. C., W. R. Holland, and J. H. S. Chow, 1978: A description of numerical Antarctic Circumpolar Currents. <u>Dyn. Atmos. Oceans</u> , <u>2</u> , 213-291.	19
6.	Rhines, P. B., 1977: The dynamics of unsteady currents. <u>The Sea</u> , Vol. 6, E. D. Goldberg, I. N. McCave, J. J. O'Brien, and J. H. Steele, Eds., Wiley Interscience, 189-318.	31
7.	Harrison, D. E. and A. R. Robinson, 1978: Energy analysis of open regions of turbulent flows - Mean-eddy energetics of a numerical ocean circulation experiment. <u>Dyn. Atmos. Oceans</u> , <u>2</u> , 185-211.	47
8.	Harrison, D. E., 1979: Eddies and the general circulation of numerical model gyres: an energetic perspective. <u>Rev. Geophys. Space Phys.</u> , <u>17</u> , 969-979.	53
9.	Haidvogel, D. B. and W. R. Holland, 1978: The stability of ocean currents in eddy-resolving general circulation models. <u>J. Phys. Oceanogr.</u> , <u>8</u> , 393-413.	61
10.	Hart, J. E., 1974: On the mixed stability program for quasi-geostrophic ocean currents. <u>J. Phys. Oceanogr.</u> , <u>4</u> , 349-356.	67
11.	Semtner, A. J., Jr., and W. R. Holland, 1978: Intercomparison of quasi-geostrophic simulations of the western North Atlantic circulation with primitive equation results. <u>J. Phys. Oceanogr.</u> , <u>8</u> , 735-754.	71
12.	McWilliams, J. C. and G. R. Flierl, 1979: On the evolution of isolated, nonlinear vortices. <u>J. Phys. Oceanogr.</u> , <u>9</u> , 1155-1182.	77
13.	Ikeda, M., 1981: Eddies detached from a jet crossing over a submarine ridge using a simple numerical model. (Submitted to <u>J. Phys. Oceanogr.</u> ), 49 pp.	87

18 Apr 1981

Summary #1 by Harley E. Hurlburt

Haidvogel, D. B., 1979: A discussion of certain modeling factors which influence the results of eddy-resolving ocean circulation studies. Dyn. Atmos. Oceans 3, 181-190.

This paper is philosophical in nature and discusses six problem areas concerning eddy-resolving ocean models (EGCM's). Haidvogel notes that the complexity of EGCM behavior and the relatively small number of EGCM simulations have frustrated attempts to adequately determine EGCM dependence on model parameters and assumptions. Such important aspects of EGCM behavior as gross time and space scales of mesoscale eddies and the generation, propagation and extinction mechanisms that characterize them, depend on a wide variety of poorly understood physical and computational approximations.

1) Primitive equation (PE) vs. quasi-geostrophic (QG) models

Typically, QG models use ten times less computer time than do PE models due primarily to the larger time step allowed. Suggests potential value of semi-implicit time stepping for PE models. Cites two comparisons. The first is for 2-layer flat bottom models without thermodynamics (Holland and Lin, 1975 (PE) vs. Holland, 1978 (QG)). Identical equilibrium eddy statistical properties and global energy fluxes are obtained in the one case compared. In another comparison Semtner and Holland (1978) demonstrate that a 2-level QG model with linearized topography and idealized heating can be made to yield the same globally integrated circulation features (*mean* transport, global loss of mean energy to the eddy field, etc.) as the 5-level PE experiment by Semtner and Mintz (1977).

2) Subgridscale frictional parameterization

Almost all EGCM experiments have used either Laplacian ( $A\nabla^2 v$ ) or biharmonic ( $B\nabla^4 v$ ) friction, the latter always in conjunction with bottom drag. Neither choice is based on a compelling theoretical argument. With Laplacian friction usually "A" large enough for sizeable extraction of KE is required for numerical stability. This is not the case with the more scale selective biharmonic friction, but the latter needs additional (unknown) boundary conditions. The use of biharmonic/bottom damping has become popular primarily because lateral friction in the ocean is thought to function mainly on the smallest scales as an enstrophy trap, and not as playing an essential role in the mesoscale eddy energy balance. However, when bottom friction and biharmonic friction are present and vertical diffusion is absent, the EGCM is forced towards a state characterized by efficient vertical exchange of energy by the eddies, which are thus automatically assigned a relatively important role in the lower layer dynamics.

3) No slip vs. free slip boundary conditions

These are a crucial factor determining the types of model ocean circulations that can develop, particularly along a northern boundary. The latter have been used in almost all EGCM experiments. In a double gyre EGCM experiment one might anticipate that a change to no slip would reduce eddy activity.

4) Environmental parameters

The number of EGCM experiments is insufficient to allow us to predict the effects of changing any particular parameter. Linear theory has proven to be of value in explaining some of the observed features of certain EGCM eddy fields, such as growth rate, wavelength and energy fluxes (Haidvogel & Holland, 1978).

These can vary greatly over physically meaningful ranges of environmental parameters such as layer depth ratio, and the ratio of the current width to the Rossby deformation radius. EGCM flow fields may evolve toward states of minimum instability.

5) Bottom topography

In EGCM studies this role has not been investigated. The effects of large scale features and of bottom roughness are of interest. The latter typically tends to decorrelate the deep circulation from the upper-layer flows and should be investigated to determine its effects on the distinctive eddy-induced deep mean flows that are driven in flat-bottom EGCM's.

6) Numerical solution technique

Haidvogel et al (1980) compared second order finite difference, fourth order finite element, and infinite-order pseudo-spectral QG barotropic models. In their experiments the fourth-order and infinite-order codes were approximately 4 and 15 times more accurate, respectively, than the second-order scheme, for fixed expenditures of computer time. Flierl (1978) has shown how to calibrate layered models so as to optimally reproduce the continuously stratified result and has shown that this depends strongly and for 2-layer models incompatibly on the physical influences present. However, two-mode models (in which the vertical dependence is expressed as a severely truncated summation of vertical eigenmodes) can be optimally calibrated for all three physical processes simultaneously.

Haidvogel concludes by suggesting some research topics involving EGCM's.

### REFERENCES

- Flierl, G., 1978: Models of vertical structure and the calibration of two layer models. Dyn. Atmos. Oceans, 2, 341-381.
- Haidvogel, D. B. and Holland, W. R., 1978: The stability of ocean currents in eddy-resolving general circulation models. J. Phys. Ocean., 8, 393-413.
- Haidvogel, D. B., A. R. Robinson, and E. E. Schulman, 1980: The accuracy, efficiency, and stability of three numerical models with application to open ocean problems. J. Comput. Phys., 34, 1-53.
- Holland, W. R., 1978: The role of mesoscale eddies in the general circulation of the ocean: Numerical experiments using a wind-driven quasi-geostrophic model. J. Phys. Oceanogr., 8, 363-392.
- Holland, W. R. and L. B. Lin, 1975: On the generation of mesoscale eddies, their contribution to the oceanic general circulation. J. Phys. Oceanogr., 5, 642-669.
- Semtner, A. J., Jr., and Holland, W. R., 1978: Intercomparison of quasigeostrophic simulations of the Western North Atlantic circulation with primitive equation results. J. Phys. Oceanogr., 8, 735-754.
- Semtner, A. J., Jr., and Mintz, Y., 1977: Numerical simulation of the Gulf Stream and mid-ocean eddies. J. Phys. Oceanogr., 7, 208-230.

Robinson, A. R., D. E. Harrison, and D. B. Haidvogel, 1979:  
Mesoscale eddies and general ocean circulation models. Dyn. Atmos. Oceans, 3,  
143-180.

This is a review paper on EGCM's, eddy resolving general circulation models of the ocean. It is a useful primer on the subject but rather superficial and degraded by extraordinarily poor proofreading. It does contain a useful catalog of 20 EGCM experiments and the basic results from them. This includes a pictorial comparison of results from different papers. The authors claim the catalog is nearly complete up to the time of the paper.

The paper begins by presenting some basic observational data on mesoscale eddies. For example, it presents a picture of eddy potential energy density for the Atlantic and notes that observations show a spectral peak for mesoscale eddies in the deep water of 50-100 days. Next the authors distinguish between process models and EGCM's. They define EGCM's as high-horizontal resolution closed-basin ocean models, driven by smooth and steady gyre-scale thermal and/or mechanical forcing functions in which mesoscale motions may occur spontaneously via internal processes as the equations are integrated forward in time. Process models assume statistical dynamical equilibrium for mesoscale variability is determined locally, although the source of the energy may not be local. They are concerned with the influence of environmental parameters such as nonlinearity, bottom topographic interactions, the  $\beta$ -effect, stratification and local friction on the properties of the eddy field. They commonly assume spatial homogeneity, periodic boundary conditions, and spin down from an appropriate initial state. For example, process models have been used to study the competition between 2-D turbulence and planetary waves introduced by the  $\beta$ -effect (Rhines, 1975), the conversion via nonlinear interaction of baroclinic to barotropic energy and its eventual migration to low wave numbers (Rhines, 1977b; Salmon, 1977) and the role of bottom topography in impeding the tendency towards purely barotropic flow, and in generating mean zonal currents by systematic pressure forces associated with bottom roughness (Rhines, 1977a; Bretherton and Haidvogel, 1976).

The EGCM's model an entire ocean basin. The dominant flow features they exhibit are a western boundary current, an eastward flowing northern boundary current or mid-latitude free jet (depending on the wind-stress and geometry chosen) and a relatively strong recirculation system associated with the eastward flowing current. The region of most intense eddy activity is almost always found in or near the eastward current and/or its recirculation. No clear preference for barotropic, baroclinic, or mixed instability processes is found. Simplified (4-box) energy box diagrams are compared for eight of the numerical experiments.

The authors contend that to understand the dynamics of the model systems, detailed analyses of the subregions and features are necessary. In fact, the global energy analyses can be misleading. In one case studied in detail the spatial inhomogeneity of the processes results in a basin-integrated energetic balance that holds for none of the energetically interesting subregions. The authors mention the usefulness of linearized stability analyses of time mean and instantaneous EGCM currents have been partially successful in identifying and characterizing localized regions of strong mean to eddy energy transfer (Haidvogel and Holland, 1978).

The EGCM experiments discussed in this paper are from Holland and Lin (1975) (2-layer primitive equations rigid lid), Han (1975) (5-level primitive equation rigid lid), Robinson, et al (1977) (5-level primitive equation rigid lid), Semtner and Mintz (1977) (5-level primitive equation rigid lid) and Holland (1978) (2-layer quasi-geostrophic rigid lid). Domain sizes ranged from 1000 km x 1000 km to 4000 km x 4000 km with 20 to 40 km grid resolution per variable. Free slip boundary conditions were used in all but one of the 20 numerical experiments. All but two experiments were for flat-bottom oceans. Semtner and Mintz (1977) included a simple shelf-slope parallel to their northwestern boundary.

#### REFERENCES

- Bretherton, F. P. and Haidvogel, D. B., 1976: Two-dimensional turbulence above topography. J. Fluid Mech., 78, 129-154.
- Haidvogel, D. B. and Holland, W. R., 1978: The stability of ocean currents in eddy-resolving general circulation models. J. Phys. Oceanogr., 8, 393-413.
- Han, Y.-J., 1975: Numerical simulation of mesoscale ocean eddies. Ph.D. Dissertation, UCLA, California, 154 pp.
- Holland, W. R., 1978: The role of mesoscale eddies in the general circulation of the ocean: Numerical experiments using a wind-driven quasi-geostrophic model. J. Phys. Oceanogr., 8, 363-392.
- Holland, W. R. and L. B. Lin, 1975: On the generation of mesoscale eddies and their contribution to the oceanic general circulation. J. Phys. Oceanogr., 5, 642-669.
- Rhines, P. B., 1975: Waves and turbulence on a  $\beta$ -plane. J. Fluid Mech., 69, 417-443.
- Rhines, P. B., 1977a: The dynamics of unsteady currents. The Sea, Vol. 6, E. D. Goldberg, I.N. McCave, J. J. O'Brien, and J. H. Steele, Eds., Wiley Interscience, 189-318.
- Rhines, P. B., 1977b: Cascades in baroclinic eddy fields. Theory and Modeling of Ocean Eddies. P. B. Rhines, Ed. Contribution of the U. S. Delegation to the Yalta POLYMODE Theoretical Institute, U.S.P.M.O.C., Dept. of Meteorology, M.I.T., Cambridge, Massachusetts.
- Robinson, A. R., Harrison, D. E., Mintz, Y., and Semtner, A. J., 1977: Eddies and the general circulation of an idealized oceanic gyre: A wind and thermally driven primitive equation numerical experiment. J. Phys. Oceanogr., 7, 182-207.
- Salmon, R., 1977: Two-layer quasi-geostrophic turbulence in a simple special case. Geophys. Astrophys. Fluid Dyn., 10, 25-52.
- Semtner, A. J. and Y. Mintz, 1977: Numerical simulation of the Gulf Stream and mid-ocean eddies. J. Phys. Oceanogr., 7, 208-230.



Holland, W. R., 1975: Energetics of baroclinic oceans. Numerical Models of Ocean Circulation, National Academy of Sciences, Washington, D.C., pp. 168-177.

This is an early paper on the energetics of coarse grid ocean model experiments using the Bryan (1969) model. It should be of only marginal interest to those currently studying the eddy-mean energetics of the ocean circulation. Many of the experiments discussed here approach a steady state and the energetics are not divided into mean and eddying parts, but are divided into external and internal modes.

The energy equations are formulated. For a closed basin the kinetic energy (KE) equation has the form

$$E_{jt} = N_j + B_j + W_j + D_j$$

where  $j = e, i$  for the external and internal modes, respectively, and  $E_t$  is the time rate of change of KE. The right hand side is the work per unit area on the mode in question by (N) the nonlinear terms, (B) the pressure or buoyancy forces, (W) the wind stress, and (D) the dissipative forces. Holland notes that  $N_e + N_i = 0$ , and shows that  $B_e = 0$  for a flat-bottom or a homogeneous ocean. Both baroclinicity and non-flat bottom topography are required for a link between potential energy (PE) and the external mode KE.

The equation for the time rate of change of PE in a closed basin is

$$P_t = -B + M$$

where M is the work per unit area by vertical and horizontal diffusion of heat and by convective mixing. Thus, B describes the conversion between PE and KE and does not affect the total energy of the system.

Holland applies these energetics to several cases. For a flat bottom ocean where nonlinearity is not important,  $E_e$  is isolated from  $E_i$  and P and it is driven by the wind alone. In the presence of variable bottom relief and stratification one of Holland's numerical experiments showed that  $B_e$  supplied 5 times as much to  $E_e$  as the wind. In fact he found  $E_i \rightarrow P \rightarrow E_e$ . With thermohaline driving only he found  $P \rightarrow E_e$  and  $E_i$  with 3 times as much going to  $E_e$  as  $E_i$ . In both cases  $N \approx 0$ . Holland also discusses dissipation time scales. Finally, Holland discusses the seasonally varying open basin energetics of the Cox (1970) Indian Ocean experiment.

REFERENCES

Bryan, K., 1969: A numerical method for the study of ocean circulation.  
J. Comput. Phys., 4, 347-376.

Cox, M. D., 1970: A mathematical model of the Indian Ocean. Deep-Sea Res.,  
17, 47-75.

Holland, W. R., 1978: The role of mesoscale eddies in the general circulation of the ocean-Numerical experiments using a wind-driven quasi-geostrophic model. J. Phys. Oceanogr., 8, 363-392.

1. Introduction. This is one of the most important papers on the dynamics and energetics of mesoscale ocean eddies to date and should be considered essential reading for anyone interested in this subject matter. In the late 60's and early 70's general circulation models of the oceans used coarse grids and high eddy viscosities. Thus, the spontaneous development of mesoscale eddies in these models was prevented. These models attempted to parameterize effects of the eddies with explicit diffusion. In models that explicitly resolve mesoscale eddies, fundamental hydrodynamic-thermodynamic laws determine the proper role played by eddies by producing fluxes of momentum and heat in various parts of the ocean circulation. The first eddy resolving numerical experiments of the general ocean circulation (EGCM's) were those of Holland and Lin (1975 a,b). Holland claims that the use of a quasi-geostrophic model in this paper is a new approach for ocean modeling.

2. Main points addressed in the paper. The eight numerical experiments in this paper are designed to examine several aspects of the general ocean circulation problem including:

1. Comparison of quasi-geostrophic (QG) and primitive equation (PE) results.
2. Comparison of single gyre and double gyre results. The Gulf Stream extension is a free jet in the latter, but not in the former.
3. Comparison of results with different frictional dissipation formulations.
4. Preliminary examination of the dependence of the results on the principal non-dimensional parameters of the problem. Holland considers these to be the Rossby number,  $Ro = \pi \gamma_0 / H_1 \beta L^3$ , the ratio of the internal radius of deformation to the basin width,  $\gamma = (g' H_1 H_3 / f_0 H)^{1/2} / L$ , the ratio of the scale for bottom friction to the width of the basin,  $W_s / L = \epsilon / \beta L$ , and to a lesser extent the layer depth ratios,  $\delta_1 = H_1 / H$ ,  $\delta_3 = H_3 / H$ , where

$\tau_0$  is the wind stress amplitude,  $H_1$  and  $H_3$  are layer thickness for the upper and lower layer,  $H = H_1 + H_3$ ,  $\beta$  is the variation of the Coriolis parameter with latitude,  $L$  is the basin width,  $g'$  is the reduced gravity ( $g \Delta\rho/\rho$ )  $f_0$  is the Coriolis parameter, and  $\epsilon$  is the coefficient for linear bottom friction.

Some important dynamical questions addressed by this paper are

1. How is downward propagation of energy accomplished?
2. Does it occur locally or over broad regions of the ocean?
3. What are some dynamical signatures for these mechanisms, especially those which could be observed in the real ocean?

3. Model Design. In this investigation Holland uses the simplest possible model to investigate the time dependent behavior of the major ocean current system in the North Atlantic. The model is two-layer, quasi-geostrophic (QG), rectangular closed basin, and has a flat bottom. Holland discusses the formulation and solution of the model equations which are pretty standard. He references Phillips (1956) and Pedlosky (1964) concerning the quasi-geostrophic formulation. Pedlosky (1979) is also an excellent reference for this. The paper discusses eight QG experiments on single gyre (1000 km by 1000 km) or double gyre (1000 km by 2000 km) domains. The grid resolution is 20 km and the numerical experiments are integrated from rest to statistical equilibrium for several years to over a decade. Holland notes that the two-layer QG model is 10 times faster than the two-layer rigid lid PE model of Holland and Lin (1975a) and 50 times faster than the five-level rigid lid PE model of Semtner and Mintz (1977). Some of the basic model parameters are  $H_1 = 1$  km,  $H_3 = 4$  km,  $g' = .02$  cm/sec<sup>2</sup>,  $\beta = 2 \times 10^{-11}$  cm<sup>-1</sup> sec<sup>-1</sup>. The boundary conditions are kinematic and free slip.

4. Rational for frictional formulation. When and only when free slip boundary conditions are used Holland conjectures that with lateral friction alone, there must be significant energy at higher wavenumbers for dissipation to balance energy input. When bottom friction is present, energy can be dissipated in the lower layer at the mesoscale eddy scale and lateral friction need play little role in the dissipation. Holland notes that Charney (1971) showed that in a turbulent, three-dimensional quasi-geostrophic flow, there is an enstrophy cascade to high wavenumbers, but there is no significant energy cascade in that direction. Thus, he conjectures that bottom friction is the primary dissipation mechanism and the general ocean

circulation is rather insensitive to the exact nature of lateral frictional processes, which operate only to dissipate enstrophy at the highest wave-numbers allowed by the model grid. Although it is not known with certainty that the larger scales have little sensitivity to the details of the high wavenumber enstrophy dissipation, Holland prefers to construct models which have as few physical processes as possible and to include only those which are most plausible at this stage. If bottom friction is important in baroclinic oceans, then the eddy processes must come into play to transport energy input by the wind downward from the surface.

The reason for using biharmonic friction rather than Laplacian is mainly computational. Biharmonic friction is more scale selective, allowing horizontal friction to act only on the smallest scales. For a given grid resolution biharmonic friction thus allows the model to exhibit smaller eddies than Laplacian, while controlling the unwanted growth of the shortest waves. This allows the model to make more efficient use of the available grid resolution. With grid resolution of 20 km, the smallest eddy viscosity which allows stable computation using Laplacian friction still produces significant damping at the mesoscale eddy scale.

5. Methodology of analyzing the results. The eddy-mean energetics are an important tool for analyzing the results of the numerical experiments. Holland discusses their formulation and the interpretation of the variables and the terms in the equations in terms of energy reservoirs and energy transfers, respectively. He then constructs energy box diagrams to represent these. Some of the types of analyses used are

1. Energy box diagrams
2. Domain energy vs. time
3. Energy transfers such as  $\overline{KE}_1$ , to  $\overline{KE}_3$  vs time
4. Plots of  $\psi_1, \psi_3, \bar{\psi}_1, \bar{\psi}'_3, \psi'_1, \psi'_3, \bar{\psi}_1 - \bar{\psi}_3$  ( $\text{eck}$ ),  $H_1 \bar{\psi}_1 + H_3 \bar{\psi}_3$  (total transport), where  $\psi$  is the streamfunction and  $h$  is the interface deviation from the mean.
5. Phase plots of  $x$  vs.  $t$  and  $y$  vs.  $t$  for a given latitude or longitude. These are used to show such things as upper and lower layer phase relations, wavelengths, speeds of propagation, and spatial variations in eddy structure.
6. Spectra at a point.
7. Zonally averaged eddy statistics vs. latitude such as,  $KE'_1$  to  $PE'$ ,  $KE'_1$  to  $KE'_3$ ,  $\overline{u'_1 v'_1}$ ,  $\overline{u'_3 v'_3}$ , and  $\overline{u'_3}$ . These curves indicate such things as the nature of instabilities vs. latitude and whether or not the eddies feed or dissipate the meanflow at different latitudes.

6. Results from the model experiments. Experiment #1 - Single gyre with Laplacian friction and an eddy viscosity of  $A = 330 \text{ m}^2/\text{sec}$ . An important purpose of this QG experiment was comparison with a comparable PE experiment by Holland and Lin (1975a). Holland found the behavior was nearly identical in this case in terms of region and nature of the physical instability, eddy space and time scales, energy levels, and energy transfers. Holland shows that energy transfers  $K_1 \rightarrow K_3$  and  $P \rightarrow K_3$  cannot exist in this model when the flow is steady. This implies there is no motion in the lower layer without the eddies. The eddies are an essential catalyst for energy transfer from  $\bar{KE}_1$  to  $\bar{KE}_3$ , the principal forcing for the lower layer in this experiment. However, lateral dissipation is the dominant energy transfer in this experiment, not transfers via the eddy field. Wind energy goes into  $\bar{KE}_1$ . Seventy-eight percent is directly dissipated by lateral friction; the remainder participates in eddy generating processes. The eddy-mean energetics indicate a predominant baroclinic instability. The tendency of the upper layer eddies to lag behind lower layer eddies in a region of instability as they propagate westward is consistent with a baroclinic instability. Outside the region of instability, the eddies are nearly barotropic. The baroclinic eddies propagate westward at 6.2 km/day and exhibit an east-west wavelength of 425 km. A plot of  $\bar{u}'\bar{v}'$  vs. latitude shows the eddy stresses tend to retard the westward return circulation.

Experiment #3 - Double gyre with Laplacian friction and  $A = 100 \text{ m}^2/\text{sec}$ . In the double gyre experiments the eastward flowing jet is highly barotropically unstable. This dominates the baroclinic instability of the weaker return flow. In the single gyre experiments the northern boundary tended to stabilize the eastward jet. There is a 47 day oscillation in the upper layer of the jet, and a 50 day oscillation in the lower layer. Seventy percent of the energy input by the wind participates in eddying processes. Since the eddies are an essential catalyst for  $\bar{KE}_1$  to  $\bar{KE}_3$  conversion, the eddies are indirectly responsible for the deep abyssal gyres even though the Reynolds stresses in the lower layer are on the average extracting energy from the mean flow in this case. The eddies tend to accelerate the eastward jet and to retard both westward return branches.

Experiment #4 - Double gyre with  $A = 2600 \text{ m}^2/\text{sec}$ . The flow becomes steady with no motion in the lower layer. In this and all the eddying experiments the time-averaged stream function is essentially anti-symmetric about the latitude of zero wind curl. However, in this case the mean gyres are elongated in the north-south whereas in the eddying cases they are elongated

in the east-west.

Experiment #5 - Double gyre with biharmonic friction ( $B = 8 \times 10^9 \text{ m}^4/\text{sec}$ ) and bottom friction ( $\epsilon = 10^{-7} \text{ sec}^{-1}$ ). The purpose was to determine the nature of the flow when bottom friction is the basic dissipative mechanism rather than lateral friction. Eight-six percent of the energy input by the wind goes into the eddy field, 10% into bottom friction and 4% into lateral friction. Except for dissipation all the energy conversions are in the same direction as in experiment #3. The mean field patterns are also similar. In both 3 and 5 upper layer eddy KE is concentrated near the jet and is due mostly to meandering of the current.  $KE'_3$  is more spread out, especially with Laplacian friction.

Experiment #6 - Double gyre with bottom friction only. The solution became computationally unstable due to the undissipated enstrophy cascade.

7. Comparison with observations shows that the model abyssal eddy energy of experiment #3 does not fall off from the maximum with latitude as rapidly as observed. This suggests the need for bottom roughness and/or bottom friction. The distribution of  $\bar{u}_3$  with latitude agrees quite well with observations.

8. Summary of results. The fundamental results are that the upper layers of the ocean are accelerated by wind and thermohaline forces acting at the surface until critical values of horizontal and vertical shears are reached. The mesoscale eddies arise spontaneously due to barotropic or baroclinic instabilities in the ocean currents. Which type of instability is dominant in the real ocean is unknown. Interaction of eddies and the mean flow shows that eddies determine the character of the large scale mean flow. The eddies propagate energy downward and limit the amplitude of the mean flow in the upper ocean. The downward energy propagation creates eddies and mean gyres in the lower layer which are an important part of the vertically averaged transport. The bottom Ekman layer acting on the eddy field is the ultimate energy sink.

9. Unanswered questions. It is not known to what extent transient wind forcing, the basin shape, the type of lateral boundary conditions, bottom topography, and thermal forcing would alter these results. For example, they may be important in determining where the current separates from the western boundary. The bottom topography may alter some of the stability conclusions in a fundamental way by changing the stability characteristics of the flow, by causing

different vertical distributions of eddy energy, and by hindering the horizontal propagation of energy (e.g., see Bretherton and Karweit, 1975; Rhines, 1977; Bretherton and Haidvogel, 1976). Also, the thermohaline component can enhance the vertical shears in the western boundary current.

## REFERENCES

- Bretherton, F. P. and D. B. Haidvogel, 1976: Two-dimensional turbulence above topography. J. Fluid Mech., 78, 129-154.
- Bretherton, F. P. and M. Karweit, 1975: Mid-ocean mesoscale modeling. Proc. Durham Conf. Numerical Methods Oceanogr., Nat. Acad. Sci., Washington, D.C.
- Charney, J. G., 1971: Geostrophic turbulence. J. Atmos. Sci., 28, 1087-1095.
- Holland, W. R. and L. B. Lin, 1975a: On the origin of mesoscale eddies and their contribution to the general circulation of the ocean. I. A preliminary numerical experiment. J. Phys. Oceanogr., 5, 642-657.
- Holland, W. R. and L. B. Lin, 1975b: On the origin of mesoscale eddies and their contribution to the general circulation of the ocean. II. A parameter study J. Phys. Oceanogr., 5, 658-669.
- Pedlosky, J., 1964: The stability of currents in the atmosphere and the ocean. Part I. J. Atmos. Sci., 21, 201-219.
- Pedlosky, J., 1979: Geophysical Fluid Dynamics. Springer-Verlag New York, 624 pp.
- Phillips, N. A., 1956: The general circulation of the atmosphere: A numerical experiment. Quart. J. Roy. Meteor. Soc., 82, 123-164.
- Rhines, P. B., 1977: The dynamics of unsteady currents. The Sea, Vol. 6, Wiley, 1048 pp.
- Semtner, A. J. and Y. Mintz, 1977: Numerical simulation of the Gulf Stream and mid-ocean eddies. J. Phys. Oceanogr., 7, 208-230.

Bil

SUMMARY #5 by Harley E. Hurlburt

McWilliams, J. C., W. R. Holland, and J. H. S. Chow, 1978: A description of numerical Antarctic Circumpolar Currents. Dyn. Atmos. Oceans, 2, 213-291.

1. Introduction. This paper represents the current state of the art on modelling the Antarctic Circumpolar Current (ACC). The six numerical solutions presented here have also probably been subjected to more different types of analysis than any others in oceanography. Papers on multiple numerical experiments have typically presented the results experiment by experiment (e.g. Holland, 1978; Holland and Lin, 1975b), dynamical topic by dynamical topic (e.g. Hurlburt & Thompson, 1980), or with a descriptive discussion followed by a dynamical one (e.g. Hurlburt and Thompson, 1976). McWilliams et al have chosen to present the results from their six numerical experiments in parallel analytical method by analytical method. For those interested in the ACC, the result is an excessively lengthy paper lacking in forward thrust. The reader must wade through many pages searching for gems of insight. Considering the length of the paper and the extent to which the numerical solutions have been analyzed, he may be disappointed in what he is able to learn about the ACC. For those interested in the methodology of analyzing numerical solutions from eddy resolving ocean models, the paper is a goldmine. The paper is organized so that the results for each type of analysis are clearly presented and easily found. Since the methodology of analysis is the primary value of the paper, we will concentrate on that aspect, making a catalogue of the techniques, saying a little about the results from each. The section numbers in the summary correspond to those in the paper.

McWilliams et al contend that the major ocean current systems only weakly interact, and hence it is reasonable to study the ACC in isolation. The plausibility of the model results tend to indirectly confirm this. The first eddy-resolving general ocean circulation model (EGCM) studies (Holland and Lin, 1975a,b) showed

that eddies develop spontaneously from instabilities in the ocean currents and in turn provide significant Reynolds stresses on them. A two-layer wind-driven quasi-geostrophic (QG) model with minimal explicit diffusion processes is the simplest and most fundamental to use in such studies. The authors emphasize that the large number of analyses of the numerical solutions performed here are intended to describe the solutions, not completely explain them. They suggest that developing simpler analogs of the behavior is perhaps the most useful approach to understanding. They cite Rhines (1975), Bretherton and Haidvoogel (1976), Salmon et al. (1976), and McWilliams (1977a) as examples. The six numerical experiments reported here are only intended to survey various processes and geometrical constraints which influence the ACC. A proper parametric study would require the identification of the possible physical regimes and documentation of the nature of the transitions between them.

## 2. The model equations, some budgets for them, numerical solution techniques.

The model is two layer wind-driven QG with important bottom friction and weak (biharmonic) lateral friction. The authors point out that layers and levels are indistinguishable in a QG model and reference McWilliams (1977b) for a derivation of the QG equations for a multiply connected domain. Since the ACC is zonally periodic, the southern boundary (continent of Antarctica) is treated as an interior island. In a closed domain the stream function ( $\psi$ ) is the same at all boundary points. In this case they must differ at the northern and southern boundary in a manner which properly reflects the transport between them. The boundary conditions are thus:

$$\psi_i = c_{iN}(t) \quad \text{on the northern boundary}$$

$$\psi_i = c_{iS}(t) \quad \text{on the southern boundary}$$

$$\nabla^2 \psi_i = \nabla^4 \psi_i = 0 \quad \text{on solid walls.}$$

where  $i=1, 3$  for the upper and lower layers, respectively. Four auxilliary conditions are required, one to determine each  $c$  at each time step. Except for the determination of the  $c$ 's, the numerical integration of the QG model (discussed in Appendix A of the paper) is pretty standard. A capacitance matrix technique Buzbee et al (1971) is used in the solution of the Poisson and Helmholtz equations when a meridional barrier representing the Drake Passage is inserted.

The formulation of the eddy-mean energetics is presented. The authors point out that two of the energy exchanges between energy reservoirs included by Holland (1978) are partially redundant in a QG model, but not in a primitive equation model. Hence, they consider seven rather than nine exchanges between the reservoirs. The authors also divide the mean energetics into zonal average and standing eddy components. The section concludes with a presentation of equations for zonal momentum and potential vorticity budgets.

3. The design of the six numerical experiments for the ACC. The basic model parameters are  $L_y = 1000 \text{ km}$ ,  $H_1 = 1 \text{ km}$ ,  $H_3 = 4 \text{ km}$ ,  $f_0 = 1.1 \times 10^{-4} \text{ sec}^{-1}$ ,  $\beta = 1.4 \times 10^{-11} \text{ cm}^{-1} \text{ sec}^{-1}$ ,  $y_0 = 500 \text{ km}$ ,  $g^t = .02 \text{ m/sec}^2$ ,  $A_4 = 10^{-7} \text{ m/sec}$ ,  $\epsilon = 10^{-1} \text{ sec}$ ,  $y_s = 220 \text{ km}$ ,  $y_n = 530 \text{ km}$ ,  $\Delta y_{\text{gap}} = y_n - y_s = 310 \text{ km}$ ,  $\Delta x = \Delta y = 19.6 \text{ km}$ ,  $\Delta t = 2 \text{ hrs}$ ,  $\tau_0 = 1 \text{ dyne/cm}^2$ , where  $L_y$  is the N-S extent of the channel,  $H_1$ ,  $H_3$  are upper and lower layer thickness,  $f_0$  is the Coriolis parameter at  $y_0$ ,  $f = f_0 + \beta(y - y_0)$ ,  $y_0 = \frac{1}{2}L_y$  is the reference latitude,  $g^t$  is reduced gravity,  $A_4$  is the coefficient of biharmonic friction,  $\epsilon$  is a coefficient of bottom friction which implies a 120 day spindown time,  $y_s$  and  $y_n$  define the northern and southern boundaries of the Drake Passage,  $\Delta x$  and  $\Delta y$  are grid increments,  $\Delta t$  is the time step for the numerical integration, and  $\tau_0$  is the amplitude of the wind stress function. The resulting internal radius of deformation is 36km. The six numerical experiments are defined in the following table.

	$L_x$ (km)	$\Delta y_{\text{gap}}$ (km)	$\alpha$ (dyne/cm <sup>2</sup> )	$B$ (m)
CH-channel flow	1000	1000	0	0
SB-small basin	1000	310	0	0
LB-large basin	2000	310	0	0
WW-weak transient wind	2000	310	.33	0
SW-strong transient wind	2000	310	.67	0
TB-topographic barrier	2000	310	0	500

$L_x$  is the E-W extent of the domain,  $\alpha$  is the amplitude of a semi-annual wind component superimposed on the mean, and  $B_0$  is the amplitude of the topographic barrier in the Drake Passage. In TB,  $B_0$  was chosen so that the topographic Rossby number ( $B_0/H_3$ ) was small enough to be quasi-geostrophic, but large enough so that  $f/(H_3)$  contours were closed in the vicinity of the minimum depth. A sufficient condition for insuring this is  $B_0 > B_0 H_3 / f_0$  ( $= 400 \text{ m}$  in this case). In reality the amplitude of the barrier in the Drake Passage is 2000m.

In the first experiment the geometry is zonally uniform. In all the others a meridional barrier representing the Drake Passage was inserted. Additional effects considered are the E-W extent of the basin, a superimposed semi-annual wind component, and a topographic barrier in the Drake Passage. Each numerical experiment was integrated to statistical equilibrium for 4 to 12 years. Only the statistically steady solution for each experiment is studied.

4. Plots of streamfunction, time averaged streamfunction, standing eddy streamfunction, streamfunction variance, and time and zonally averaged zonal velocity. The eddies have scales much larger than the radius of deformation about 100 to 200km with wavelength of 400-800km. The eddy scales seem similar to that of the horizontal shear of the zonal jet. The standing eddies are zonally uniform in SB, LB, and SW and have virtually the same wavelength, which is wavenumber 1 in SB, wavenumber 2 in LB and SW. The standing eddies in TB are spatially inhomogeneous. The topography nearly eliminates the zonal jet in the lower layer, a strong feature of the other 5 experiments. Except for TB, the solutions are nearly equivalent barotropic (i.e. same patterns in upper and lower layer, but different in strength with larger velocities in the upper layer). In TB mean gyres north and south of the jet rotate in directions prescribed by a Sverdrup balance ( $y_0$  is a line of zero wind curl). The greatest streamfunction variance in all cases is <sup>in</sup> the vicinity of the jet. Except in case CH, substantial local maxima are associated with non-propagating oscillations in the amplitude of the instantaneous standing eddies.

5. Energetics. The authors start by plotting the total and eddy energy for each case vs time. Curves for potential energy and kinetic energy in each layer are plotted. Scale analysis of the energy integrals shows PE>KE should be expected when the dominant current scale is greater than the radius of deformation. In the flat bottom cases there is no phase lag between KE & PE, but KE lags PE in TB. The authors are able to offer no explanation for a striking 3 year oscillation in the TB case.

The eddy-mean energy box diagrams indicate a baroclinic instability in all the flat bottom cases. Baroclinic instability is defined as  $\bar{P} + P'$  (mean potential energy to eddy potential energy) being the dominant mean to eddy transfer. There

is also a reverse instability in the upper layer,  $K'_1 \rightarrow \bar{K}_1$ . The mean zonal-standing eddy energy box diagrams show the primary source of the standing eddies is a barotropic instability,  $K_{1z} \rightarrow K_{1*}$ , where the subscript, z, is for the time and zonal mean and \* is for the standing eddy component based on the difference between the time mean, and the time and zonal mean streamfunction. In the SW case no significant work is done on the fluid by the transient wind. This implies an almost complete lack of correlation between forcing and response. The TB case is one of mixed instability,  $\bar{P} \rightarrow P' \approx \bar{K}_1 \rightarrow K'_1$ . The primary source for the standing eddies is a baroclinic instability. An upper layer barotropic instability and a topographic conversion are lesser sources of standing eddy energy. All of the transient eddy exchanges with the time and zonal mean are reverse instabilities.

6. Transport through the Drake Passage is plotted vs time for each case. Observations show a transport of 100-200 Sv. SB, LB, SW show 400-600 Sv with more in the lower layer than the upper. TB shows 30 to 60 Sv in the upper layer and -60 to 10 Sv in the lower layer with a slightly negative mean in the lower layer. In the SW case the variation in transport (300 Sv peak to peak) is strongly correlated with the wind with little lag. However, plots of  $\Psi_1$  vs time near the center of the basin show no clear relation to the wind.

7. The transient solutions are examined in this section using (1) time series of  $\Psi_1'$ ,  $\Psi_3'$ ,  $v_1'$ ,  $v_3'$  at a point, (2) spectra at a point, (3) propagation (Hovmöller) diagrams of  $\Psi_1$ ,  $\Psi_3$ , and  $\Psi_1 - \Psi_3$ , (4) principal component plots using empirical orthogonal functions, and (5) times series of principal component amplitude. The primes denote eddy components and v is the meridional component of velocity. The authors use Davis (1976) as a reference for the principal component analysis.

In the LB case a 40-60 day period is evident which is consistent with a mean jet advection period of  $2\pi l/U$  where  $U=30$  cm/sec and  $l=150-250$  km. In the TB case a longer 90-130 days period is observed, perhaps due to the slower jet. The 3 year period in energy and transport through the Drake Passage is not evident in the time series of  $\Psi_1$  at the center of the basin, but is weakly evident in spectra.

A plot of x vs t for  $\Psi_1$  at a central latitude of case LB showed contour slopes in regions of strong gradient give a propagation speed of 30-35 km/day and a wavelength of 850 km for eddies. This implies a period of 24-28 days, shorter than in the time series or spectra. Because the regions of strong gradient do not typically persist long compared to a period, it is clear that a single period or phase speed is insufficient to characterize the field. Individual eddy centers

do not persist long enough to propagate across the entire domain. Thus, the simple description of mean jet advection of passive spatial structures is inadequate, even though useful for estimating the magnitude of phase speeds and periods. The authors find substantial differences between the upper and lower layer phase speeds even though individual eddy centers are correlated between layers. This reflects the fact that many of the eddy centers are nearly stationary. There is little systematic propagation in case TB. Eddy behavior in this case has little to do with mean current advections.

A principal component analysis is performed using empirical orthogonal functions. The principal components with the largest eigenvalues are the most efficient, statistically independent (with respect to the time average) description of the variability of the  $\Psi$  field. For principal components of  $\Psi$  that are geostrophically balanced, the principal components of the velocity components are redundant. As an example, the authors apply the principal component analysis to case CH. Seven <sup>Components</sup>  $\wedge$  explain 88% of the variance and correspond to one standing and three propagating patterns. Time series of the amplitude of the principal components reveal periods which correspond to peaks in the spectra. Coherence between the time series of two similar patterns shows propagation. The principal components provide a succinct summary of the variability of the solutions, but why particular components are present, their dynamical couplings, and their coupling with the mean jet, the driving, and the dissipation remains unanswered.

8. Zonal momentum budgets show that the Reynolds stresses by the transient eddies tend to concentrate mean eastward momentum at the center of the jet in the upper layer by accelerating the center and retarding the periphery of the jet. Essentially, this is because barotropic planetary waves transport westward momentum (Kuo, 1951). If an instability, say, produces these waves at the center of the jet, then they leave behind eastward momentum as they propagate out of the jet and subsequently deposit westward momentum in an exterior region. The deposition process is probably associated with near-critical layers (Dickinson, 1968, 1971). The interfacial pressure drag by the eddies is the primary momentum source for the lower layer, sink for the upper layer. In the lower layer the momentum sink is bottom friction or in case TB topographic pressure drag. The downward transfer of zonal momentum by the transient interfacial pressure drag is equivalent to the downward transfer of mean energy, i.e.  $\bar{K}_1 \rightarrow \bar{P}$ .

9. Potential vorticity is the most fundamental dependent variable in a QG model in many respects, since it is a conservative property of a fluid parcel except for dissipation and the wind driving. The potential vorticity budgets show that horizontal transport of eddy relative vorticity is a local jet source (for potential vorticity stronger than the wind) while the vertical stretching due to eddies is a sink to the lower layer. In cases CH, SB, SW, and LB transient eddies and in case TB standing eddies are most important in this regard. The potential vorticity source for the lower layer (eddy stretching) is balanced by bottom friction, except in TB by bottom topography torque. The eddy relative vorticity transport weakly tends to spread the jet in the lower layer.

For cases considered here, purely steady solutions to the model equations would be those where standing eddies could effect all the transports which are necessary in the energy, momentum, and vorticity budgets. To the extent that point balances are dominated by conservative forces, the model equations approximately collapse to

$$J(\bar{\Psi}_i, \bar{q}_i) = 0 \quad (1)$$

in a steady solution. This equation has a general solution of the form  $\bar{q}_i = f(\bar{\Psi}_i)$ . This relation was tested by plotting  $\bar{q}_i$  vs  $\bar{\Psi}_i$  for all points on the model grid in a scatter diagram for each experiment. All but case TB showed a nearly single valued relationship, implying a near solution to (1). The largest departures occurred on the solid meridional boundaries where  $\bar{\Psi}_i \neq f(y)$ , but where  $\bar{q}_i$  varies due to  $H_i \delta y$ . McWilliams (1977a) showed that quasi-geostrophic stability of mean states approximately satisfying (1) is assured by

$$\frac{d\bar{q}_i}{d\bar{\Psi}_i} > 0$$

everywhere in each layer. Here, this is generally true in the lower layer for CH, SB, LB, and SW, but not in the upper layer for any case. The transient eddies are associated with the slight non-uniqueness of the relation between  $\bar{q}_i$  and  $\bar{\Psi}_i$ .

10. Eddy properties and fluxes in case CH. Because of the relative simplicity of this case, a more precise analysis of the eddy properties is possible. This section investigates the relation between linear instability theory and the numerical principal components, the momentum transports by each component, the validity of some parameterizations of eddy heat flux, the degree of supercriticality of the mean state of case CH, and the role of the reverse energy cascade ( $K_1$  to  $K_1'$ ),

which is analogous to that of two-dimensional turbulence.

The linear stability analysis is like that of Haidvogel and Holland (1978). Wavenumbers 2 and 3 are found to be unstable with wavenumber 3 by far the most unstable. For wavenumber 2 the wavelength is 500km, the period is 14 days, and the e-folding growth time is 550 days. For wavenumber 3 the wavelength is 333km, the period is 9 days and the e-folding growth time is 87 days. This agrees fairly well with spectral peaks and the results of the principal component analysis. However, the stability analysis predicts greater energy flux divergence per unit streamfunction amplitude in wavenumber 3 than does the principal component analysis. Wavenumber 2 has 16 times the streamfunction variance of wavenumber 3, even though the linear stability analysis predicts a 6 times smaller growth rate.

It is useful to compare the flux divergence contributions to the general circulation from the unstable modes (wavenumbers 2 and 3) and from the principal components. This was done in terms of the zonal mean momentum transports, although other mean budgets could have been used. When contributions from the first 20 principal components were evaluated, it was found that only two propagating pairs contributed significantly, the two which corresponded to the linearly unstable modes. However, these principal components account for only 17% of the total streamfunction variance. Since the linear theory does not suggest that any of the other, more energetic, principal components can be generated by an instability of the mean state, and since the others are generally unimportant in the mean budgets, the authors conclude that there must be an efficient energy cascade from the unstable modes to other components; predominantly a reverse cascade to larger scales as in two-dimensional turbulence (see Batchelor, 1969). However, the cascade does not make the flow more barotropic (as described by Rhines, 1977), apparently due to the presence of the vertically sheared mean jet.

Stone (1978) parameterized heat flux based on the hypothesis that the heat flux is that which is required to maintain the time and zonal mean vertical shear in the velocity near the value for marginal instability. The authors verify marginally supercritical mean flow for case CH.

11. Theories of the ACC. The authors discuss some historical theoretical ideas about the ACC and show that the numerical solutions support a vertical eddy viscosity of about  $1\text{m}^2/\text{sec}$  and a horizontal eddy viscosity of  $1000$  to  $2000\text{m}^2/\text{sec}$ .

12. Summary of results for the model ACC's. The numerical solutions illustrate the nature of the equilibrium turbulent balances between geostrophic eddies and mean jets which are strongly coupled. The eddy-mean energetics show that the transient eddies are generated by a baroclinic instability of the mean jet, except in case TB where the instability is mixed barotropic/baroclinic. Using a linear stability analysis, two spectral peaks in case CH at 9 and 20 days were shown to result from baroclinic instability. The horizontal scales were much larger than the radius of deformation. Other more energetic transient motions receive energy via a reverse cascade similar to that of 2-D turbulence.

The fundamental horizontal scale of the system is set by the strength of concentration of the mean, meridional potential vorticity gradient. The eddies act to intensify the upper layer mean jet and mean cross-jet potential vorticity gradient primarily through horizontal Reynolds stresses and relative vorticity flux divergence, respectively. Because of this up-gradient momentum flux, the jet is narrower in the upper layer than the lower layer. There is a downward transfer of mean zonal momentum, energy and potential vorticity gradient through interfacial pressure drag, vertical pressure work, and vortex stretching flux divergence, respectively.

The partial meridional barrier and the topographic obstacle in the Drake Passage strongly influence the equilibrium solution, but it is quite insensitive to the change in E-W basin length or to the addition of a semi-annual wind component to the mean. The meridional barrier introduces energetic standing eddies. When the topographic barrier is added, many aspects of the flow are altered quite drastically. The mean standing eddies dominate the zonal mean. Closed gyres with a partial Sverdrup balance are present both north and south of the jet. The flow is much more energetic downstream than upstream of the topographic barrier. The transports and energies are greatly reduced, the transports from more to less than observed. The mean transport in the lower layer is even weakly negative (reversed). The eddy-mean energetics indicate a mixed barotropic/baroclinic instability. The standing eddies, not the transient, contribute most to interior fluxes in the zonal mean momentum and potential vorticity budgets. Topographic drag and torque serve as major sinks rather than bottom friction. The authors express frustration at their inability to explain a prominent 3 year

oscillation in case TB, without presenting any plausible or implausible explanations. Thus, they don't say why they rule out an internal Rossby wave excited through the initialization and early spin-up.

Appendix B discusses relations among eddy fluxes which appear in the mean momentum, energy, and vorticity budgets.

## REFERENCES

- Batchelor, G. K., 1969: Computation of the energy spectrum in homogeneous two-dimensional turbulence. Phys. Fluids Suppl., 12(II), 233-239.
- Bretherton, F. P. and Haidvogel, D. B., 1976: Two dimensional turbulence above topography. J. Fluid Mech., 78, 129-154.
- Buzbee, B. L., F. W. Dorr, J. A. George, G. H. Golub: The direct solution of the discrete Poisson equation on irregular regions. SIAM J. Numer. Anal., 8, 722-736.
- Davis, R. E., 1976: Predictability of sea surface temperature and sea level pressure anomalies over the North Pacific Ocean. J. Phys. Oceanogr., 6, 249-266.
- Dickinson, R. E., 1968: Planetary Rossby waves propagating vertically through weak westerly wind wave guides. J. Atmos Sci., 25, 984-1002.
- Dickinson, R. E., 1971: Cross-equatorial eddy momentum fluxes as evidence of tropical planetary wave sources. Quart. J. Roy. Meteor. Soc., 97, 554-558.
- Haidvogel, D. B., and W. R. Holland, 1978: The stability of ocean currents in eddy-resolving general circulation models. J. Phys. Oceanogr., 8, 393-413.
- Holland, W. R., 1978: The role of mesoscale eddies in the general circulation of the ocean - Numerical experiments using a wind-driven quasi-geostrophic model. J. Phys. Oceanogr., 8, 363-392.
- Holland, W. R. and L. B. Lin, 1975a: On the origin of mesoscale eddies and their contribution to the general circulation of the ocean. I. A preliminary numerical experiment. J. Phys. Oceanogr., 5, 642-657.
- Holland, W. R. and L. B. Lin, 1975b: On the origin of mesoscale eddies and their contribution to the general circulation of the ocean. II. A parameter study. J. Phys. Oceanogr., 5, 658-669.
- Hurlburt, H. E. and J. D. Thompson, 1976: A numerical model of the Somali Current. J. Phys. Oceanogr., 6, 646-664.
- Hurlburt, H. E. and J. D. Thompson, 1980: A numerical study of Loop Current intrusions and eddy shedding. J. Phys. Oceanogr., 10, 1611-1651.
- Kuo, H.-L., 1951: Dynamical aspects of the general circulation and the stability of zonal flow. Tellus, 3, 268-284.
- McWilliams, J. C., 1977a: On a class of stable, slightly geostrophic mean gyres. Dyn. Atmos. Oceans., 1, 19-28.

- McWilliams, J. C. 1977b: A note on a consistent quasi-geostrophic model in a multiply-connected domain. Dyn. Atmos. Oceans, 1, 427-441.
- Rhines, P. B., 1975: Waves and turbulence on a  $\beta$ -plane. J. Fluid Mech., 69, 417-443.
- Rhines, P. B., 1977: The dynamics of unsteady currents. The Sea, 6, 189-318.
- Salmon, R. L., G. Holloway, and M. C. Hendershott, 1976: The equilibrium statistical mechanics of simple quasi-geostrophic models. J. Fluid Mech., 75, 691-704.
- Stone, P., 1978: Baroclinic Adjustment. J. Atmos. Sci., 35, 561-576.

11 June 1981

## SUMMARY #6 by Harley E. Hurlburt

Rhines, P. B., 1977: The dynamics of unsteady currents. The Sea, Vol. 6, E. D. Goldberg, I. N. McCave, J. J. O'Brien, and J. H. Steele, Eds., Wiley Interscience, 189-318.

### 1. Introduction

This is a major article which should be studied by anyone seriously interested in the dynamics of the mesoscale and large scale ocean circulation at mid-latitudes, despite some frustrations which the reader will probably encounter. The paper emphasizes that mesoscale ocean eddies exhibit quasi-geostrophic dynamical features of both waves and turbulence, particularly three types of Rossby waves and two-dimensional quasi-geostrophic turbulence. These two aspects are then used to elucidate the dynamical behavior of mesoscale eddies and unsteady currents in a variety of situations. This summary is organized to make use of the headings and subheadings of the original paper.

### 2. Historical Introduction

Rhines asserts that the kinetic energy of the oceans takes on four dominant forms: surface waves, near inertial and tidal oscillations, the climatological mean circulation, and unsteady currents with periods greater than 1/2 pendulum day. The latter, especially quasi-geostrophic mesoscale eddies ( $\sim 200$  km) are the focus of the paper. Sections 2-5 discuss some classical ideas, 6-9 some new or recently published material.

A. Observational history. Although there were earlier hints, the mesoscale variability of the open ocean really began to be appreciated only in the 1950's through the work of people like Stommel, Fuglister, Swallow, Crease, and Worthington.

B. Dynamical background. Eddies in the atmosphere and ocean are approximately the same size when scaled by the internal radius of deformation  $L_p$ , and the speeds are similar when scaled by  $BL_p^2$ . However, some important differences in the dynamics will be pointed out later. Certainly the inhomogeneity in the ocean circulation is much greater than in the atmosphere.

### 3. Kinematics of Eddy Fields

A. Space. Integration smooths and differentiation roughens a field. Successive differentiation in space corresponds to high pass filtering.

The breadth of the spectrum determines the extent to which this filtering affects it. As one proceeds from relatively narrow to white spectra, differentiation has a greater and greater effect. Three important characteristics of a spacial spectrum are the centroid,  $k_1$ , the breadth,  $k_2$ , and the slope of the asymptotic tail,  $\sim k^{-N}$ .

#### B. Scales.

C. Time. Similarly for temporal spectra, the centroid frequencies,  $\omega_1$ , breadth,  $[(\omega - \omega_1)^2]^{1/2}$ , and slopes of spectral tails,  $\sim \omega^{-N}$  are important.

D. Dynamics. The slope of the asymptotic tail can show if there is sufficient dissipation at small scales to actively damp the energy containing eddies. In violently energetic 3-D turbulence the slope  $\sim k^{-5/3}$ , so the spectrum is broad enough for this to occur, but in flows like geostrophic turbulence we have  $k^{-3}$  and the spectra are too sharp to be dominated this way by friction. Rhines points out the importance of the spectral gap between the eddies and the inertial-tidal-internal wave motions. Since the frequency and wavenumber spectral amplitudes decrease  $\sim \omega^{-3}$ ,  $k^{-3}$  above the spectral peak for the eddies, the local energy cascade to inertial/wave motions is blocked. The spectral gap in the atmosphere is much less severe.

#### 4. Dynamics of the Gentlest Kind

This section is concerned with a class of flows that occurs when forcing is so gentle that fluid columns can resist vertical stretching and compression. In a homogeneous fluid where nondimensional frequency,  $\omega$ , Rossby number,  $\epsilon$ , and Ekman number,  $E$ , are all small, we get the Taylor-Proudman approximation. As  $\omega \rightarrow 0$ , energy propagation becomes increasingly vertical, painting out Taylor columns and the group velocity,  $c_g \rightarrow fL$ , where  $f$  is the Coriolis parameter and  $L$  is a horizontal length scale, here that of the Taylor column. The time for this propagation approaches  $h/fL$  where  $h$  is the depth of the fluid. Since the energy propagation in this situation is so rapid, the fluid columns are quite rigid and free motions must be directed along constant  $f/h$  contours, so that the fluid columns are not strained vertically.

A. Hough, Goldsbrough, Sverdrup flow. Now consider a gentle downward motion,  $w_0$ , imposed at the upper surface, perhaps due to Ekman convergence. To avoid vertical compression and obey continuity,  $w = w_0$  throughout the column and the fluid columns must move toward greater values of  $f/h$ . The velocity normal to these contours is  $v = w_0 \beta H/f$ , where  $H$  = mean depth. Assume  $w_0$  is due to Ekman convergence, then

$$\beta v = \frac{\text{curl} z^T}{\rho_0 H}$$

With rough bottom topography and horizontally non-divergent flow, this generalizes to

$$h \vec{u} \cdot \nabla(f/h) = \frac{\text{curl} z^T}{\rho_0 H}$$

Note free geostrophic flows would still follow  $f/h$  contours.

B. Stratification. A Sverdrup balance can also exist for internal modes, with flow confined entirely to the upper layer of a two-layer flow in the steady state. However, the time scale for the setup of internal mode Sverdrup flow is so long that it is easily disrupted locally by unsteady forcing, etc.

C. Time dependence (low frequency). Rhines derives the nondispersive internal Rossby wave of Veronis and Stommel (1956) which propagates with speed  $c_0 = \beta L_p^2$ , where  $L_p$  is the internal radius of deformation. He presents the example of a wind distribution turned on slowly at time  $t = 0$  designed to generate an anti-cyclonic circular vortex. The flow is initially barotropic, but intensifies in the upper layer and vanishes in the lower as a transient mirror image vortex moves to the west as an internal Rossby wave with current speeds in the vortex  $v_2/v_1 = H_1/H_2$  (Lighthill, 1969). With topography the baroclinic wave speed is increased to one that approaches  $c_0(1 + H_1/H_2)$  and the lower layer is nearly at rest. Strong bottom friction,  $E^{1/2} \gg \beta L_p^2/fL$ , also speeds up the propagation and brings the lower layer flow to rest while causing vanishingly small dissipation.

D. Spherical geometry. If forcing becomes so rapidly changing that less work is expended when the flow allows some vertical stretching with less meridional motion, then the Sverdrup flow gives way to Rossby waves,

and the existence of relative vorticity becomes essential. If the forcing is so intense that nonlinearity is significant ( $BL^2/U < 1$ ), then the linear waves give way to two-dimensional quasi-geostrophic turbulence. Note  $U$  is a velocity scale and  $L$  is an associated length scale.

## 5. Linear Potential Vorticity Waves

The scale of the most energetic eddies in the ocean is  $\sim 100$  km. Even though these eddies are strongly nonlinear, vestiges of linear theory apply well into the nonlinear range, e.g., the group velocity of low frequency waves provides some upper bound guidance on the rate at which influence can propagate laterally.

A. Derivation of equations in non-dimensional form. The primitive equations are expanded in the Rossby number,  $\epsilon$ , to derive an equation for conservation of geostrophic potential vorticity. Also mentioned are a barotropic potential vorticity law which includes the role of topography and Ertel's (1942) relation which defines a potential vorticity that is conserved even in strongly ageostrophic inviscid flows.

B. Linear waves. Rhines discusses three types of linear Rossby waves derived from the quasi-geostrophic potential vorticity equation when the wave steepness,  $\epsilon/\omega \rightarrow 0$ , where  $\omega$  is the wave frequency normalized by the Coriolis frequency,  $f$ :

1. a barotropic Rossby wave, which for scales greater than the internal radius of deformation,  $L_p$ , is also valid with a topographic effect added.

2. a bottom trapped wave with a simple buoyancy oscillation for a dispersion relation. If the N-S bottom slope exceeds that of  $\beta(\sim 10^{-3})$ , this high frequency wave may be expected at scales  $\leq L_p$ .

3. a mode which has an oscillatory vertical structure, the non-dispersive internal Rossby wave. With realistic stratification, it tends to be confined to the upper ocean where stratification is the greatest. A fraction of the wave energy,  $\sim (L/L_p)^2$  is potential. For a flat bottom the greatest N-S component of the group velocity is  $.23 BL_p^2$ .

C. Initial value problems.

D. Observations of oceanic signals resembling the linear waves are presented. Rhines notes the significance of the fact that the fast, long, weak westward propagating Rossby waves reflect at a western boundary into slow, short, strong eastward propagating waves.

6. Nonlinear Waves and Turbulence: Primary Cascades

This section gives a new treatment of nonlinear cascades that occur in a flat-bottom ocean when the wave steepness,  $\epsilon/\omega$  is not small. Rhines measures this in terms of the ratio of the fluid particle speed to the theoretical phase speed and notes that it is typically  $\geq 0(1)$  for all three types of linear quasi-geostrophic Rossby waves, suggesting strong nonlinear interactions between Fourier components. In fact at oceanic energy levels energy may travel faster through wavenumber space than physical space, in the sense that significant horizontal and vertical eddy-eddy interactions can occur before propagation has moved the energy a single wavelength.

A. The diagram for a flat-bottom ocean. For nearly linear waves the wave interactions are slow. When nonlinearity is important, there is a general movement of baroclinic flows toward the internal deformation radius,  $L_p$ , for both larger and smaller scale flows. This scale is then an aperture through which energy passes downward from slowly propagating baroclinic to more swiftly propagating barotropic motions. After this there is expansion toward larger scale (linear) barotropic motions, an adjustment toward states near the transition between waves and quasi-geostrophic turbulence. This is the theme which will be amplified in succeeding subsections.

B. Barotropic cascade. There is a red shift of the centroid  $k_1$ , as an initially narrow energy spectrum spreads out due to nonlinear wave interaction. This can lead to a negative eddy viscosity in terms of westerly momentum. Enstrophy exhibits a mean shift to higher wavenumbers. However, unlike 3-D turbulence, the 2-D enstrophy cascade is too slow to form an inertial subrange which carries energy efficiently to small scales for viscous dissipation.

C. Obstacles to the red cascade of barotropic eddies:

1. Isolation of eddies - When eddies are too isolated to interact as turbulence, then they no longer exhibit the 2-D cascade to larger scales.

2. As a red cascade proceeds, the flow becomes more linear. As linearity is approached, the wave interaction and red cascade are greatly slowed.

D. Anisotropy. With  $\beta$  present eddies become elongated E-W, perhaps even to the point of becoming zonal bands. This may be anticipated by noting that weak wave interactions seem to cascade predominantly to lower frequencies, while 2-D turbulence tends to cascade toward low wavenumbers. The latter implies higher frequencies for barotropic Rossby waves, if we fix the ratio of the N-S and E-W scales.

E., F., G. Baroclinic cascades. Studies with a two-layer model show that for scales  $> L_p$  the layers are strongly coupled by interfacial motion and attendant vortex stretching. At scales  $\ll L_p$ , the coupling is negligible and the interface effectively becomes rigid, separating two decoupled barotropic layers. However, if small eddies ( $< L_p$ ) in the upper layer are non-linear enough so that they can exhibit a red cascade to  $L_p$  before becoming linear, then when they reach that scale they can communicate effectively with the lower layer. As the interface is deformed vorticity of the same sign develops in the other layer and potential energy is then effectively converted to kinetic. From this point the behavior is like the barotropic cascade described in Subsection 6B. These results complement the geostrophic turbulence theory of Charney (1971) which also shows a cascade to both larger horizontal and vertical wavenumbers. In this cascade ellipses expand in size but maintain the same eccentricity. Once the flow becomes barotropic this can no longer be true.

Linear baroclinic eddies with  $L \gg L_p$  would propagate westward as non-dispersive internal Rossby waves at speed  $\beta L_p^2$ . However, large baroclinic eddies are baroclinically unstable and quickly break down into eddies with scale  $\sim L_p$ . To violate the red cascade in the horizontal with baroclinic instability, the motion must evolve toward larger vertical scales to compensate for the growth of smaller horizontal scales. Based on the total wavenumber (horizontal and vertical) the cascade is still red. Baroclinic instability is the primary nonlinear effect in large baroclinic eddies.

In a numerical experiment large eddies ( $L \gg L_p$ ) initially confined to the upper layer showed local episodes of baroclinic instability with eddies developing on scales  $\sim L_p$ . The flow then tended toward barotropy and the scales again increased. This eventually resulted in a fairly barotropic

zonally dominated flow. The baroclinic instability augments the anisotropic effects discussed earlier. (1) Meridional flows are more unstable and break down into preferentially zonal eddies (zonal perturbation currents are unopposed by  $\beta$ ). (2) There is a finite amplitude eddy-eddy induction of zonal flow to be discussed in Section 8. If the zonal configuration develops soon enough, then vertical shear,  $\Delta U$ , can remain and is stable if  $\beta L_p^2 / \Delta U > 1$  (approx.); i.e., the zonal configuration can defeat the potential enstrophy cascade, which is a prerequisite for barotropy.

H. Meanders in a two-layer Gulf Stream. Rhines uses a periodic two-layer model with an initial eastward zonal jet in the upper layer to model the Gulf Stream extension. The half width of the jet is  $\sim L_p$  and  $\beta = 0$  so  $\beta L_p^2 / U = 0$ . Rhines uses the model to illustrate some of the dynamics discussed previously and to show that it is able to depict some features of the observed Gulf Stream. A meandering instability occurs in the upper layer in  $< 20$  days and eddies form in the lower layer. Rhines points out that deep motion and its phase shift (leading the perturbations overhead) are known to be essential to baroclinic instability. Eventually the growing eddies become sufficiently nonlinear to interact with each other (instead of just with the mean flow). Eddies of like sign in the lower layer begin to coalesce and create an eastward zonal mean abyssal flow and the scale of the eddies increases.

I. Energy-transfer spectra. Wave-wave interactions are computed from Fourier transforms of the various advective terms in the potential vorticity equation. At scalar wavenumber,  $k$ , this interaction takes the form

$$\frac{\partial(K+P)}{\partial t} = T_\psi(k) + T_P(k) + T_H(k) - D(k)$$

where  $K$  is kinetic energy,  $P$  is available potential energy,  $T_\psi(k)$  is due to relative vorticity advection in both layers,  $T_P(k)$  to density advection,  $T_H(k)$  to bottom topography, and  $D(k)$  to various types of friction. The conversion between  $K$  and  $P$  at a single wavenumber is given by

$$C_{PK}(k) = T_P - \frac{\partial P}{\partial t} .$$

A numerical experiment showed that at first  $T_p$  carried energy away from the centroid mostly toward higher wavenumbers (baroclinic instability). Near the internal deformation radius  $P$  was converted to  $K$ . Then  $T_\psi$  transported the energy back to small wavenumbers, although it acted in this direction throughout the experiment. The flow eventually became nearly barotropic. Rhines also comments on extension of the results to the case with multiple vertical levels.

## 7. Basins and Bottom Topography

One flaw in the previous results is that the development toward barotropy is far more rapid than is consistent with the ocean. Topography and sidewalls act as sources of enstrophy to counter or grossly alter several of the nonlinear cascades, and to alter the nature of the horizontal propagation.

A. Coastal boundaries with free slip. The red cascade can be reversed near a western boundary. Recall that with linear Rossby waves, western wall reflection converts long waves to short, increasing the enstrophy. Since the small scale motions propagate slowly, this favors the concentration of both energy and enstrophy in the west, and their removal from the eastern ocean. In a two-layer ocean, both potential energy release within the body of the fluid and energy at its western periphery can increase the enstrophy and move the centroid of the energy spectrum to large wavenumbers.

B. Rough bottoms. Rhines discusses the inclusion of topography in a two-layer quasi-geostrophic (QG) model. Depth variations are included only in the vortex stretching term of the potential vorticity equation. Thus, topographic heights ( $\sim H_2 \delta$ ) must be limited to order Rossby number ( $\delta \leq \varepsilon$ ) or nondimensional frequency ( $\delta \leq \omega$ ) whichever is larger, where  $H_2$  is the mean thickness of the lower layer and  $\delta$  is the RMS height of the topography normalized by  $H_2$ . Rhines chooses bottom slopes such that planetary and topographic Rossby waves would have comparable amplitude. Also topographic scales  $< L_p$  are eliminated.

C. Effect on the primary nonlinear cascades. Sufficiently intense flows ( $\varepsilon \gg \delta + L_H/R$ , where  $R$  is the radius of the earth and  $L_H$  is the horizontal scale of topography with a single scale) act as 2-D turbulence, but as flows become gentler, the topography can generate relative enstrophy, increasingly

fragmenting large eddies into small ones, and countering the red cascade of 2-D turbulence. However, it is necessary to consider topography of more than a single length scale, since spectral broadening occurs when energy at wavenumber  $k$  interacts with topography at wavenumber  $\mu$ , producing energy at wavenumber  $k \pm \mu$ . Typically, topography has a nearly white (flat) spectrum ( $\sim k^{-2}$ ) which quickly whitens the energy spectrum, favoring a transfer to large wavenumbers. In a stratified ocean, topography can affect the vertical structure as well as the horizontal, countering the nonlinear tendency to direct energy toward large vertical scales in the interior. As shown in Section 8, the degree of openness of the  $f/h_2$  contours is crucial to the processes of horizontal propagation and mean-flow induction. Here the effects of topography on deformation scale eddies, very large eddies, and linear waves will be considered.

D. Deformation-scale eddies. With the topography described and initial deformation scale eddies of moderate energy, the barotropic mode becomes a stable vertical structure only at scales  $>> L_p$  and the overall transition to barotropy is prevented. The thermocline eddies dominate the upper level currents and the thermocline height, and propagate westward at nearly the internal Rossby wave speed. However, at higher energy levels the behavior is the same as in the flat-bottom case, with eddies interacting vertically, tending toward barotropy, then expanding horizontally, and developing anisotropy and  $f/h$  contour flow.

The vertical structure of the flow which develops depends on  $\epsilon/\delta$  and  $\beta L_p^2/U \equiv \epsilon L_p/R$ . For eddies with scale,  $L \sim L_p$ , the equilibrated flow is increasingly barotropic as  $\epsilon/\delta$  increases. Numerical experiments show that topographic control of the vertical structure (preservation of vertical shear) occurs when  $\epsilon/\delta \leq .5$  within about a  $500 \times 500$  km region. For eddies with  $L >> L_p$ , this dependence on  $\epsilon/\delta$  is much less. When  $\beta L_p^2/U$  is large (implying linearity), the flow does not become barotropic even in the absence of topography and the RMS velocities obey  $U_2/U_1 \approx H_1/H_2$ . When the flow is nearly linear, there is trapping of fast waves in the deep water and slow waves in the shallow water, just as in linear theory. In the spectral transfer functions  $T_H$  (due to topography) greatly augments  $T_p$  in transferring energy to higher wavenumbers, but with  $T_\psi$  still transporting energy to lower wavenumbers. Generally, topography whitens the wavenumber spectrum for energy, whereas the nonlinear cascades, by themselves, tend to sharpen it.

E. Initially large-scale eddies contain more P than K. Recall that with a flat bottom, first conversion to the deformation scale via baroclinic instability is the dominant nonlinear process, followed by conversion of P to K as the flow becomes barotropic, followed by a (reverse) cascade back to larger scales via 2-D turbulence. When topography is added, the conversion of P to K is greatly suppressed by the inhibition of barotropy, even though this conversion is initially greater (due to horizontal scattering by topography which must release P at high wavenumbers, since small eddies can't contain much P). Also with topography (unlike with a flat bottom) some P to K conversion is possible with a linear flow.

The process of baroclinic instability is intrinsically different with rough topography, even when f/h contours are still open. This is a result of spectral broadening by the roughness, which carries energy continuously along the k-axis rather than having it leap to the deformation radius,  $L_p$ . At scales  $\gg L_p$  the flow still tends toward barotropy and develops an anisotropic (zonal) character as in the flat bottom case.

F. Fine structure, anisotropy, mean flows. The lower layer flow tends to become more heterogeneous over rough topography and to follow f/h contours. There is a tendency for persistent anticyclonic gyres above seamounts. Both western boundaries and topography tend to increase the relative enstrophy of the flow.

G. Lateral propagation of energy in the ocean is of great interest because of the sparse distribution of really active energy sources in the ocean and because of the great size of the ocean compared to that of the  $O(L_p)$  scale of the energetic eddies. Linear, flat-bottom theory is inadequate for understanding this, since nonlinearity and topography can quickly affect the propagation and the mix of vertical modes. The nonlinear effects contrive doubly to increase the group velocity, first by switching the eddies to the vertical mode with fastest propagation, and then by expanding the horizontal scale of the eddies. The topography reduces the lateral propagation by inhibiting the switch of vertical modes, by topographic backscatter, by trapping some energy over closed f/h contours, and by transporting energy to higher horizontal wavenumbers.

H. The linear wave problem and small-scale topography. The parameter  $\epsilon/\delta$  discriminates between nonlinear cascades over flat or rough bottoms. Significant topography with a single dominant scale,  $L_H$ , tends to induce fluid motions

near that scale with frequency  $\delta f$ , so that  $\epsilon/\delta = U/f\delta L_H$  is the ratio of the current speed to the phase speed. It also measures the extent to which fluid crosses an entire topographic feature during a wave period ( $\pm 2\pi$ ). When the excursions measured this way are small, the waves can be treated as linear and there may be an approach to quasi-steady Taylor columns/cones. Observations show that flows in the deep water shift so often that steady, potential vorticity conserving deflections are a poor description of the effects of topography. Parameterization of the effects of small-scale topography and its wave drag on mesoscale eddies is crucial. The use of linear bottom friction to do this may be severely in error.

When  $\epsilon/\delta \leq 1$  wave theory suggests some of the turbulent<sup>†</sup> cascades.

- (1) Linear scattering of long waves provides a model for  $T_H(k)$ , the topographic energy transfer spectrum, which may allow a quantitative estimate of spectral broadening and fragmentation even of non-linear eddies. (2) The occurrence of bottom trapped Rossby waves is consistent with high-frequency oscillations found only in the lower layer of the numerical simulations.
- (3) Recall that the linear barotropic wave cannot exist for scales  $\leq L_p$  when non-flat topography is present. The disappearance of this wave at  $L \leq L_p$  suggests, in the turbulent runs, the sustenance of vertical shear (defeat of barotropy), since it is the scales near  $L_p$  which form the aperture through which the different levels communicate. (4) The prediction from theory of horizontally trapped waves over rough topography is suggestive of the immobility of energy found in the nonlinear cases. This further suggests that spatial intermittency of energy and local equilibrium of the eddies should develop in both linear and nonlinear oceans.

#### 8. Mean-Flow Interaction

Steady forcing can produce unsteady currents and eddies which can affect the time or space averaged flow in which they are imbedded. Conversely, a purely oscillatory forcing can produce a rectified flow. There are many ways to define a mean flow. Due to the generalized Stokes drift, the velocity average about fixed control surfaces does not describe the average paths of fluid parcels. Oceanographers who are interested in the life history of salts, heat, momentum, and chemical tracers must also be concerned with such Lagrangian means, averaging over an ensemble of realizations. Rhines illustrates the difference between Eulerian and Lagrangian means.

A. A whole-gyre model. So far the focus has been on process models without boundaries and in which the fields are normally homogeneous. This subsection reviews the work of Holland and Lin (1975) who use a closed-basin, two-layer model with free slip boundaries which is integrated several years to statistical equilibrium. This model exhibits heterogeneous flow fields when driven by a simple, steady wind distribution appropriate for a subtropical gyre. The primary currents generated in the model are a western boundary current, an eastward northern boundary current, and a westward return current south of it. In this case meanders of the westward return current provide an explicit source of eddies which may radiate to the central ocean. The upper layer meanders in this current lag those in the lower layer by about  $60^{\circ}$ . This is a tilt of the phase of pressure in the x-z plane opposite to the sense of the mean, a familiar signature of baroclinic instability. Simple instability theory which ignores horizontal shear, suggests that for the eastward flow to be unstable  $|U_E| > g'H_2\beta/f^2$  (in order that the mean potential vorticity gradient have opposite sign in the two layers). When the upper layer is thin, the westward flow can more easily exhibit reverse gradients in the two layers, if only  $|U_W| > g'H_1\beta/f^2$ . Thus, if  $|U_W/U_E| > H_1/H_2$ , the westward return flow will be more vulnerable to baroclinic instability.

The eddies drive an abyssal circulation. Above the thermocline the mean flow is significantly weaker with eddies than without. Spontaneous wave radiation intensifies an eastward jet and weakens a westward jet. With a free eastward jet eddies should act to intensify the circulation in both layers. These remarks will be amplified in succeeding subsections. Baroclinically unstable westward currents mix heat equatorward. The distant eddy field radiated from the north is virtually barotropic. This dearth of strong thermocline eddies is in disagreement with oceanic observations, where unlike the model probably  $P > K$ . This is the same disparity found in the flat-bottom cascades. The addition of topography and reduction of lateral friction should allow baroclinic eddies in the far field. Heterogeneous numerical solutions, especially, require accurate modelling of horizontal energy fluxes, which are dependent on friction and bottom topography.

B. Rectified circulation on a homogeneous  $\beta$ -plane.

C. Inviscid theory is used to demonstrate the ability of random forcing confined to a zonal band to generate mean zonal flows with no net angular

momentum, if none is provided by the forcing. This contributes to earlier arguments for anisotropy favoring zonal or f/h currents on a  $\beta$ -plane.

D. Viscous theory is examined with a simple linear bottom drag added to the inviscid theory, such as would be provided by a linear Ekman layer.

E. Taylor's formula (1915) is used by Rhines to define a kind of eddy viscosity which can be negative in some cases. He uses it to derive Rayleigh's criterion for barotropic instability (i.e., on a  $\beta$ -plane  $\beta - U_{yy}$  must change sign at some latitude, where  $U$  is a zonally averaged velocity). This implies that westward jets are less stable than eastward jets with the same shape. During the instability the role of  $\beta$  is to cause westward acceleration of the mean flow in a broader band and eastward flow in a narrower band, than in the case with  $\beta = 0$ .  $\beta$  takes on the dominant role when  $\beta L^2/U > 1$ , where  $L$  is the horizontal scale of  $U$ .

F. Energy conversion to and from the mean flow. Rhines comments on the difficulty of distinguishing between spatial flux terms and conversions between means and perturbations.

G. Webster's experiment (1965) to measure energy flux and energy conversion in the Gulf Stream is discussed.

H. Linearized theory: momentum transport in Rossby waves. On a  $\beta$ -plane outward-moving disturbances in a basically stable flow necessarily sharpen an eastward jet and broaden a westward jet (Subsection 8E).  $\beta$  also hastens the redistribution of momentum by allowing waves to propagate. The dispersion relation for barotropic Rossby waves generated along an E-W line have crests arranged in a herringbone pattern pointed eastward. This results in a westward flux of momentum,  $uv$ , away from the source, augmenting an eastward jet at the center, but creating a westward counter-current to either side.

I. Rossby waves in a shear flow. Another approach shows that Rossby waves propagating outward from the center will augment an eastward jet and weaken a westward jet.

J. Topographic effects: nonlinear theory. Random forcing can also generate currents following geostrophic contours, f/h, including anticyclonic circulations above seamounts and ridges, and cyclonic over depressions. This

may be an important way that deep currents along continental slopes are generated. However, small scale bottom roughness probably acts as a drag (Bretherton and Karweit, 1975).

K. Applications. Among other things Rhines comments that regions receiving eddy energy should see development of mean westward flow, those losing it mean eastward flow.

## 9. Observational Notes

A. Sources of eddy energy at least include direct wind generation, violent instabilities of intense currents and radiation from them, slower instability of the gentle mid-ocean currents, flow past rough topography and irregular coastlines, occasional sinking of cold water, enhancement by western-boundary reflection, and possible driving by internal wave stresses. The sources are more sparsely distributed in the ocean than in the atmosphere and the domain is much larger in terms of deformation radii and propagation rates.

B. Dissipation by lateral friction is much weaker than suggested by classical eddy coefficients. The very nature of geostrophic turbulence, by its inability to extend vortex lines indefinitely, is to avoid such dissipation. Unlike the atmosphere the deep valley in frequency spectra between periods of a day and a few weeks shows the lack of a homogeneous cascade between geostrophic and ageostrophic flow. Again unlike the atmosphere bottom friction is very slight and suggests a spin-down time exceeding 500 days. Yet the ratio of vertically integrated kinetic energy density to the rate of working by the wind stress suggests an ocean spin-down time for kinetic energy of only 19 days. Lee wave drag by topography may be far more significant than bottom stress (Bell, 1975). The search for oceanic energy sinks is not ended.

### C. Mode: velocity

D. Zonal bands. Rhines cites some observational evidence for anisotropic (zonally banded) flows. He also comments on the higher frequency of deep flows compared to shallow flows and on the tendency for vertical coherence of the deep flow.

D. Temperature.

E. Particle paths. Neutrally buoyant SOFAR floats released at 28N, 69°40'W and 1500 m during MODE showed a typical SW drift, but with strong oscillations superimposed. The SW drift suggests Sverdrup flow with westward phase propagation. The kinetic energy seen by the floats was reduced over a region of rough topography. The tracks also show some tendency to trace out the shape of the large-scale topography.

## REFERENCES

- Bell, T. H., 1975: Topographically generated internal waves in the open ocean. J. Geophys. Res., 80, 320-327.
- Bretherton, F. P. and M. Karweit, 1975: Mid-ocean mesoscale modeling. Numerical Models of Ocean Circulation, National Academy of Sciences, Washington, D.C., pp. 237-249.
- Charney, J. G., 1971: Geostrophic turbulence, J. Atmos. Sci., 28, 1087-1095.
- Ertel, H., 1942: Ein neuer hydrodynamischer Wirbesatz. Meteorol. Z., 59, 277-281.
- Holland, W. R. and L. B. Lin, 1975: On the generation of mesoscale eddies and their contribution to the oceanic general circulation, I and II. J. Phys. Oceanogr., 5, 642-669.
- Lighthill, M. J., 1969: Dynamic response of the Indian Ocean to west of the southwest monsoon. Phil. Trans. Roy. Soc., A, 265, 45-92.
- Taylor, G. I., 1915: Eddy motion in the atmosphere. Phil. Trans. Roy. Soc., A, 240, 1-26.
- Veronis, G. and H. M. Stommel, 1956: The action of variable wind stresses on a stratified ocean. J. Mar. Res., 15, 43-75.
- Webster, F., 1965: Measurements of eddy fluxes of momentum in the surface layer of the Gulf Stream. Tellus, 17, 239-245.

15 June 1981

SUMMARY #7 by Harley E. Hurlburt

Harrison, D. E. and A. R. Robinson, 1978: Energy analysis of open regions of turbulent flows - mean eddy energetics of a numerical ocean circulation experiment. Dyn. Atmos. Oceans, 2, 185-211.

1. Introduction. Large spatial inhomogeneities exist in eddy-resolving general circulation models of the ocean (EGCM's). In numerical experiments involving these, spatially averaged budgets may not be characteristic of the dynamical behavior of any subregion and cannot yield information about the causes or effects of the spatially unaveraged structure. This paper investigates the regional energy budgets for a numerical experiment using a 5-level primitive equation model reported by Robinson et al (1977), which will be referred to as RHMS. The regional energetics help provide physically meaningful differentiation between different model flows and provide information about physical processes responsible for the flows in different regions. However, a serious interpretational difficulty is encountered in the analysis. In an open region the interaction work of the Reynolds stresses with the mean flow does not generally produce a conversion of energy between the mean kinetic energy of the eddy field (MKEF) and the kinetic energy of the mean flow (KEM), as it does in a closed region.
2. Open region energy analysis. The authors consider three time averaged energy equations for (1) KEM, (2) MKEF, and (3) mean total potential energy. The MKEF equation is the difference between the equations for mean kinetic energy and kinetic energy of the mean flow (KEM). A linear formulation of potential energy precluded division of the mean potential energy equation in a similar manner. The mechanisms responsible for the production, redistribution, and dissipation of MKEF are the primary focus of the paper. The energy equations contain three classes of processes: transport of flux, diffusion, and interaction. The divergence terms represent transport processes, the diffusive terms processes not explicitly resolved by the numerical calculation including dissipation and external driving by external stresses and heat fluxes. The interaction terms involve direct or indirect coupling of two different types of energy.

The two interaction processes considered here are buoyancy work (the interaction of the total flow with the gravitational field) and the Reynolds stress-mean flow interaction work (RS-MF). The latter are labelled based on an analogy between viscous and Reynolds stresses. Buoyancy work is responsible for conversions between KEM and mean potential energy, and between MKEF and the latter. Possible ambiguity associated with alternate forms of interaction terms must be resolved by defining specific physical processes responsible for the interactions (Lorenz, 1955). An interaction represented by the same terms with opposite sign in two energy equations is a conversion between those two forms of energy. The two buoyancy work conversions are of this form. However, the RS-MF conversion is of this form only in a closed domain. This creates a problem of interpretation for regional energetics, but one which can be reduced if a region where RS-MF is small or where it acts approximately as a conversion process can be defined.

Most of the remainder of the paper is concerned with the energy balance in the MKEF equation which is schematically represented as follows:

$$\text{TENDENCY} + \text{DIVERGENCE} + \text{RSMF} = \text{HORIZONTAL AND VERTICAL DIFFUSION} + \text{BUOYANCY WORK}$$

The divergence term is zero when integrated over a closed domain and consists of three fluxes of MKEF at the boundary of an open domain due to (1) mean flow advection, (2) mean eddy advection of eddy energy, and (3) boundary mean eddy pressure work. The authors represent the MKEF equation by a box for MKEF with an arrow pointing in or out to represent each of the terms in the equation. The tendency term is neglected since a long time average for flow in statistical equilibrium was used.

3. RHMS MKEF energy terms. The authors define the dynamical or kinematical regions of the EGCM experiment of RHMS. The major mean currents in the solution are a western boundary current, an eastward northern boundary current, and a westward return current south of the latter. The westward return current (NBCW) and a region just to the south of it are the regions of greatest eddy activity. Except for a region in the southwestern part of the basin, the remainder is termed the interior solution. The authors plot maps of the various terms and calculate energy term variances in order to perform tests of significance that they are different from zero. The maximum amplitude point values generally

pass at the 99% level. The authors also point out two regions (the NW corner and the region of separation of the northern boundary current) where the numerical solution is suspect due to numerical noise.

The authors comment on the maps of the various terms. In general they are quite inhomogeneous. RS-MF acts as an energy conversion only in the central portion of NBCW with the mean flow feeding the eddies. The RS-MF terms are also large in a surrounding region but don't balance. Overall in the basin RS-MF converts KEM to MKEF over each depth interval. The eddy buoyancy work is generally small, and except in the SW basin doesn't show a substantial region of consistent sign and large enough values to play an important role in the energy balances. The only significant dissipation or diffusion of MKEF due to vertical diffusion is through bottom stress, and it is strongest where the eddies are strongest. Horizontal diffusion work is comparable to vertical except that it is larger near the free slip boundaries of the domain.

Mean flow transport of MKEF is an efflux in the eastern part of NBCW and near the northern boundary current separation, and an influx in the central and western part of NBCW and just south of it. Point values of mean eddy flow transport of MKEF are not statistically significantly different from zero at the 95% level except in NBCW and just south of it. This is not a very important term in this simulation. The mean eddy pressure work transport of MKEF is calculated as a residual in the MKEF equation. The central part of NBCW shows a strong efflux of this term, most of the rest of the basin an influx. Outside NBCW and slightly south of it, this is the most important transport and is at least comparable even there. There is a net southward flux south of NBCW and an eastward flux transporting MKEF east of the separation of the northern boundary current.

4. Regional MKEF budgets. Using the MKEF boxes with the arrows, the authors present results for several vertically integrated regions and regional breakdowns. Cases where the RS-MF terms are important, but don't balance (so they don't represent a conversion) cloud the interpretation in some dynamically important regions. The authors attempt to alleviate this problem with some success by defining alternate regions.

5. Discussion of the main findings from the regional energetics study. A combined region consisting of NBCW and a comparably sized region just to the south of it is the primary source region for MKEF. Within it KEM

is converted to MKEF via RS-MF, about half is dissipated, and the remainder is exported via eddy pressure work. The eddy field in the interior is maintained against dissipation predominantly by influx of MKEF from eddy pressure work. The eddy field in the SW part of the basin is maintained primarily by eddy buoyancy work conversion of potential energy to MKEF. The western and northern boundary currents are rather passive as sources or sinks of MKEF in the simulation of RHMS.

The eddies do not directly drive a mean flow either in the source region or in the domain as a whole, but instead draw energy from it. The primary vertical transfer of KEM from the wind-driven surface to depth appears to be mean vertical pressure work. In the case of RHMS the vertical integration of the energetics causes no essential loss of information, especially in the primary source region. The authors criticize earlier interpretations of RS-MF by Holland and Lin (1975) and Semtner and Mintz (1977) and discuss how their interpretations would alter conclusions about the model dynamics.

## REFERENCES

- Holland, W. R. and L. B. Lin, 1975: On the generation of mesoscale eddies and their contribution to the oceanic general circulation. Parts I and II. J. Phys. Oceanogr., 5, 642-669.
- Lorenz, E. N., 1955: Available potential energy and the maintenance of the general circulation. Tellus, 7, 157.
- Robinson, A. R., D. E. Harrison, Y. Mintz, and A. J. Semtner, Jr., 1977: Eddies and the general circulation of an idealized oceanic gyre: a wind and thermally driven primitive equation numerical experiment. J. Phys. Oceanogr., 7, 182-207.
- Semtner, A. J., Jr. and Y. Mintz, 1977: Numerical simulation of the Gulf Stream and mid-ocean eddies. J. Phys. Oceanogr., 7, 208-230.

J. L.

## SUMMARY #8 by Harley E. Hurlburt

Harrison, D. E., 1979: Eddies and the general circulation of numerical model gyres: an energetic perspective. Rev. Geophys. Space Phys., 17, 969-979.

1. Introduction. Considerable attention has been focused on the possible roles of time-dependent mesoscale motions in the long-time-averaged ocean circulation. At present, questions about eddy-mean flow interaction can only be addressed using eddy resolving ocean models (EGCM's), even though they may not properly represent the real ocean. Of particular interest is the extent to which these interaction results depend on the assumed model physics, on other modeling decisions, and on the nondimensional model parameters. It is important to determine which EGCM results are general and which are experiment dependent. Energy budgets for the long-time-averaged circulation of EGCM experiments are the only widely used analysis methods that permit investigation of the eddy-mean flow interaction in the EGCM's. They allow determination of mean and eddy energy levels, the relative importance of Reynolds stresses and buoyancy processes in creating eddy flow, and the importance of the eddy source processes in the overall energy budgets. The purpose of this excellent paper is to provide a framework for the interpretation of energy budgets presently in use, a mostly nondimensional summary of the useful energy results of the published closed basin EGCM experiments, a discussion of their implications, and a discussion of some shortcomings in the present energetics analysis procedures.

2. Basin energy budget analysis is based on integrating the model energy equations over the entire closed domain. One flaw in this procedure results from the spatial inhomogeneity of the model solutions, so that local energy budgets may be quite different from the domain-averaged budget. The simplest representation of the closed-basin eddy-mean energetics consists of a 3-box diagram. Each box represents an energy equation which has been averaged in time and over the entire domain. The energy equations are for the kinetic energy of the mean flow ( $\bar{K}$ ), the mean kinetic energy of the eddy flow ( $K'$ ) and the mean potential energy ( $P$ ). Note that the mean kinetic energy equation has been divided into two parts (for mean and eddy kinetic energy) while the potential energy has not. This is because some EGCM experiments use a linear rather than

quadratic form of potential energy. Even in some cases with quadratic potential energy, nothing is gained by splitting it. Schematically, the three energy equations have the form:

$$\bar{K}_t = - RSW + MBW + \bar{F} - \bar{D} \quad (1a)$$

$$K'_t = RSW + EBW + F' - D' \quad (1b)$$

$$P_t = -MBW - EBW + F_p - D_p \quad (1c)$$

Since the energetics are calculated using long time averages and numerical solutions in statistical equilibrium, the tendency terms are neglected. The first two terms on the RHS of each equation are conversions of energy from one form to another and they are represented by arrows connecting the boxes on the energy box diagram. The conversions are Reynolds stress work (RSW), mean buoyancy work (MBW), and eddy buoyancy work (EBW).  $\bar{F}$  and  $\bar{D}$  are steady forcing and dissipation of the mean flow,  $F'$  and  $D'$  are time dependent forcing and eddy dissipation, and  $F_p$  and  $D_p$  are thermal forcing and dissipation. The  $F$ 's and  $D$ 's are represented by arrows in or out of the boxes. Harrison recommends Bird et al (1960) and Van Mieghem (1973) as useful references on energy equations.

There are several ways to measure the importance of the eddies in the energy budget. One is

$$E \equiv \frac{EBW + RSW}{\bar{F} + F_p} \quad (2)$$

where  $E$  measures the fraction of the energy put into the mean circulation that drives the eddy flow.  $EBW, RSW > 0$  indicates transfer of energy to the eddies. Other nondimensional energy measures of the importance of eddies are  $K'/\bar{K}$  and  $D'/\bar{D}$  or  $D'/(D + D_p)$ .

Equations (1) represent three equations in nine unknowns, so that six work terms are independent, the same as the number of forcing and dissipation terms. If the modeller controls these terms, then the conversion terms are determined. For example, energy measures of eddy importance can be completely determined by these processes. If  $F' = 0$ , then

$$\frac{D'}{\bar{D} + D_p} = \frac{E}{1 - E} \quad (3)$$

Thus, we see a potential importance of the physical form of the dissipation term. The only measure of eddy importance previously discussed that is not in principle determined by the dissipation is the ratio  $K'/\bar{K}$ .

Consider the steady wind/adiabatic case so that  $F_p = D_p = F' = 0$  and  $EBW = -MBW$ . In statistical equilibrium the total dissipation must balance the wind input. The solution will spin up from rest until it reaches sufficient intensity to provide this dissipation. This may be possible with a steady flow ( $K' = D' = 0$ ) or with an unstable time dependent meandering or eddying flow. Strong current instability appears to be the principal source of eddies and this depends at least on the forcing structure and amplitude, vertical resolution, viscous boundary layer width, velocity boundary conditions, and the E-W extent of the basin, all of which are determined by *a priori* model choices. However, it should be noted that the dissipation arguments do not imply any constraints on RSW/EBW (only on RSW + EBW).

3. EGCM basin energy results for 21 EGCM experiments from Holland and Lin (1975), Robinson et al (1977), Semtner and Mintz (1977), Holland (1978), Holland (unpublished), and Semtner and Holland (1978) are summarized in terms of  $\bar{K}$  and 7 ratios:  $K'/\bar{K}$ ,  $\bar{D}/\bar{F}$ ,  $D'/\bar{D}$ ,  $F_p/MBW$ ,  $\bar{BD}/HS$ ,  $BD'/HS'$ , and RSW/EBW, where BD is dissipation due to bottom stress work and HS is that due to horizontal stress work. From these it is possible to reconstruct normalized three-box energy box diagrams for each experiment.

Some of the results noted by Harrison are: (1) To a crude approximation, most of the cases suggest that beyond a mean flow intensity comparable to that required by the traditional shear instability criterion (Pedlosky, 1964), additional forcing does not increase  $\bar{K}$ . (2) A crude linear relation exists between  $K'/\bar{K}$  and  $D'/\bar{D}$ . When Laplacian friction was used,  $D'/\bar{D} < 1$ ; when biharmonic friction plus bottom drag were used,  $D'/\bar{D} > 4$ . Almost all the experiments used free slip boundary conditions. In most experiments dissipation due to horizontal and bottom friction was approximately comparable whether the horizontal friction was Laplacian or biharmonic. (3) In all 21 experiments RSW > 0, indicating a  $\bar{K}$  to  $K'$  energy transfer. In all but one EBW was also positive, transferring energy from P to  $K'$ . The values of  $|RSW/EBW|$  ranged from .07 to 25. For  $RSW > 0$  and  $RSW/EBW > 5$ , the energy source is predominantly barotropic instability, for  $EBW > 0$  and  $RSW/EBW < .2$  predominantly baroclinic instability,

and for the remaining cases with  $RSW, EBW > 0$  a mixed instability. The EGCM experiments are roughly equally divided among the three categories. The cutoff values are Harrison's, although he prefers to call them Reynolds stress work dominated or buoyancy work dominated rather than barotropically or baroclinically unstable, respectively, because the indicated energy transfers can exist in the absence of barotropic or baroclinic instability (Kuo, 1973; Green, 1970). No general dependence of  $RSW/EBW$  on a particular nondimensional number has been found, although modeling choices which narrow or strengthen the strong currents tend to increase  $RSW/EBW$  over comparable experiments, while those which concentrate the currents in the vertical tend to decrease the ratio.

4. Open region energy analysis. Because of the spatial inhomogeneity of the EGCM flows, it is important to understand the range of energetic behaviors that exist within the regions of a given flow. A general regional energy analysis must account for horizontal and vertical energy transport processes and will often confront difficulty in unambiguously defining energy conversion processes (Lettau, 1954; Harrison and Robinson, 1978). Ideally, the regional energy analysis would reveal where energy is put into the system by the forcing, transformed from one type of energy to another, transported horizontally and vertically, and lost to dissipation. So far no complete regional analysis has been performed for any EGCM experiment, but a regional  $K'$  energetics study for the experiment by Robinson et al (1977) has been reported by Harrison and Robinson (1978), and in some cases energetics have been analyzed for two or three slabs in the vertical covering the horizontal extent of the domain. This allows separate examination of the energetics of the shallow and deep flow and some of the processes responsible for vertical transport of energy. The problems of open region analysis are discussed only to the extent needed to assimilate the results of the EGCM energy budgets already reported. In particular, some differences introduced by the use of quasi-geostrophic (QG) rather than primitive equation (PE) models are examined for the case of two-layer energetics. The QG experiments have neglected vertical transfer due to vertical diffusion. They have also neglected vertical advection because the QG solutions are horizontally nondivergent to within 0 (Rossby number) and assume that vertical advection is small compared to horizontal advection. In two-layer QG models there is a single reservoir for  $P$  in the vertical because "temperature" is only

defined at one level.

The definition of vertical velocity  $w$ , in the QG EGCM models results in differences from the PE models. Combined with the layer vorticity equations, this results in the upper/lower region buoyancy work ratios in the two-layer QG models being set by the mean layer thickness ratio, i.e.,  $H_1/H_2 = EBW_1/EBW_2 = MBW_1/MBW_2$ . It is never possible to have buoyancy work transfer energy one way in the upper layer and the opposite in the lower layer. In a PE model the buoyancy work ratio is model determined and can have either sign. In fact in the case of Robinson, et al (1977), the ratio for  $EBW_1/EBW_2 < 0$ . The QG approximation may not be appropriate for the physics of the long-time-average vertical velocity field in the ocean.

If the flow is steady and adiabatic, then  $\bar{w} = 0$  and there is no flow in the lower layer (Holland, 1978). This is a result peculiar to this QG model and does not apply to a QG model with subgrid scale vertical diffusion, or to a PE model. This result has been used to assert the fundamental importance of eddies to the existence of abyssal circulations, and its lack of generality should be carefully noted.

Because of the buoyancy work ratio constraints, only six additional independent energy ratios are needed to construct a two-layer energy box diagram for the two-layer QG experiments. They are  $RSW_1/RSW_2$ ,  $D_1/D_2$ ,  $\bar{D}_1/\bar{D}_2$ ,  $H_1/H_2$ ,  $K_1/K_2$ , and  $\bar{K}_1/\bar{K}_2$ .  $K_1$  and  $K_2$  are taken to be energy densities (energy/volume) to allow the ratios to be used as measures of the baroclinicity of the mean and eddy flow. The baroclinicity of the eddy flow measured this way ranges from 1.1 to 13, and it is not correlated with  $\bar{K}_1/\bar{K}_2$ . On the average the mean flow is approximately twice as baroclinic as the eddy flow. No relationship between these ratios and the dissipation mechanism or ratio has been detected. When  $RSW_2$  is significant, it represents transfer from mean to eddies ( $\bar{K}_2$  to  $K_2'$ ), as in the upper layer, for all the QG experiments listed.

Harrison concludes the section on regional energetics with a brief summary of results from Harrison and Robinson (1978) for kinematically distinct regions of an EGCM experiment (see summary #7).

5. Summary and discussion. The basin averaged results presented in Section 3 show the importance of eddies in the EGCM experiments reported varies greatly, with  $K'/\bar{K}$  ranging from about .3 to 6, and with values of  $E$  from (2) ranging from < .1 to .9. However, two experiments with very

Similar domain averaged energetics could exhibit quite different flows. In general, the reported results behave along classical turbulence lines with the mean flow feeding the eddies. No significant negative viscosity is observed in any of the reported results, although this possibility cannot be ruled out, particularly in regional energy budgets. However, this was not found in the regional budgets by Harrison and Robinson (1978) for the numerical experiment of Robinson, et al (1977).

The domain averaging of the energetics introduces strong constraints on what can be learned from them. Regional analysis can improve the situation somewhat, but even that gives at best a mechanistic description of how energy is moved along the possible pathways, not why it moves that way. Evaluation of budgets including eddy transports of heat, momentum, and vorticity may prove more helpful in gaining dynamical insight, than evaluation of energy budgets, and they may be more easily applied to ocean data.

Much study is required to determine whether the essential physics is preserved in special model systems such as the two-layer QG and on how to interpret their results in a general context. It is clear that eddies can be important, at least as an energy pathway to dissipation, but whether this result is special to the biharmonic operator/bottom drag dissipative mechanism modeling choice requires further investigation. The use of time dependent forcing should increase the probability of eddies driving mean flows, and the introduction of bottom topography on eddy scales may fundamentally alter the behavior of the flow. The use of additional vertical transport processes in QG models should give insight into the generation of deep flows.

## REFERENCES

- Bird, R. B., W. E. Stewart, and E. N. Lightfoot, 1960: Transport Phenomena, Wiley, New York, 700 pp.
- Green, J. S. A., 1970: Transfer properties of the large-scale eddies and the general circulation of the atmosphere. Quart. J. Roy. Meteorol. Soc., 96, 157-185.
- Harrison, D. E. and A. R. Robinson, 1978: Energy analysis of open regions of turbulent flows - Mean-eddy energetics of a numerical ocean circulation experiment. Dyn. Atmos. Oceans, 2, 185-211.
- Holland, W. R., 1978: The role of mesoscale eddies in the general circulation of the ocean - Numerical experiments using a wind-driven quasi-geostrophic model. J. Phys. Oceanogr., 8, 363-392.
- Holland, W. R. and L. B. Lin, 1975: On the generation of mesoscale eddies and their contribution to the oceanic general circulation I, II. J. Phys. Oceanogr., 5, 642-669.
- Kuo, H. L., 1973: Dynamics of quasi-geostrophic flows and instability theory. Advan. Appl. Mech., 13, 247-330.
- Lattau, H. O., 1954: Notes on the transformation of mechanical energy from and to eddying motions. J. Meteorol., 11, 196-201.
- Pedlosky, J., 1964: The stability of currents in the atmosphere and the ocean, I. J. Atmos. Sci., 21, 201-219.
- Robinson, A. R., D. E. Harrison, Y. Mintz, and A. J. Semtner, Jr., 1977: Eddies and the general circulation of an idealized oceanic gyre: A wind and thermally driven primitive equation numerical experiment. J. Phys. Oceanogr., 7, 182-207.
- Semtner, A. J., Jr., and W. R. Holland, 1978: Intercomparison of quasi-geostrophic simulations of the western North Atlantic circulation with primitive-equation results, J. Phys. Oceanogr., 8, 735-754.

Semtner, A. J., Jr., and Y. Mintz, 1977: Numerical simulation of  
the Gulf Stream and mid-ocean eddies, J. Phys. Oceanogr., 7, 208-230.

Van Mieghem, J., 1973: Atmospheric Energetics, Clarendon, Oxford,  
306 pp.

17 June 1981

SUMMARY #9 by Harley E. Hurlburt

Haidvogel, D. B. and W. R. Holland, 1978: The stability of ocean currents in eddy-resolving general circulation models. J. Phys. Oceanogr., 8, 393-413.

1. Introduction. This paper uses a linear stability analysis (LSA) to investigate the barotropic and/or baroclinic instability of ocean currents simulated in the eddy-resolving (EGCM) experiments of Holland (1978). It is motivated by the observation that strong currents in the model are a spontaneous source region for mesoscale eddies, which in turn significantly modify the mean flow. In these currents both horizontal and vertical shears appear to be important, resulting in a mixed stability problem in which there is a simultaneous conversion of kinetic ( $\bar{K}$ ) and potential ( $\bar{P}$ ) energy of the mean flow to the eddies. This study also tests the relevance of linear stability analysis to the complex model results and to real ocean applications. In the model the final statistical balance between mean and mesoscale eddy fields is determined by finite-amplitude eddy-mean flow interactions, so the usefulness of the LSA is subject to question.

2. The two-layer quasi-geostrophic (QG) model of Holland (1978) is briefly described (see summary #4).

3. The eddy-resolving numerical experiments numbers 1, 3, and 5 of Holland (1978) are described, since the LSA is applied to these. Experiment 1 is a single gyre experiment with Laplacian friction, experiment 3 is a double-gyre ocean with Laplacian friction, and experiment 5 is a double-gyre ocean with bottom friction and highly scale selective biharmonic lateral friction. All three experiments use free slip boundary conditions. The biharmonic friction requires an extra tangential boundary condition which Holland (1978) applies as  $\nabla_4 \psi = 0$ .

The authors use LSA in several ways to investigate the dynamics of the numerical solutions and to test its usefulness in predicting features of the numerical solutions. (1) They determine whether the LSA can be used to predict the space and time scales of the finite-amplitude eddy field, the relative phase of the upper and lower layer eddies, and the location and size of the region of instability. (2) They investigate whether the global energetic transfers obtained from the EGCM simulations agree with

those from the LSA. (3) They attempt detailed LSA-EGCM comparisons of the meridional or zonal distribution of certain higher order eddy statistics such as eddy kinetic energy ( $K'$ ), the Reynolds stresses, and some of the energy transfer terms found to be important in the global energetics of the numerical experiments, i.e.,  $\bar{P}'$  to  $K_1'$ ,  $K_1'$  to  $K_3'$ , etc., where  $P$  is potential energy and  $K_i$  is kinetic energy in layer  $i$ . An overbar denotes energy of the mean field, a prime energy of the eddy field, and  $i = 3$  is the lower of two layers.

In experiment 1 the numerical solution shows an eddy diameter or half wavelength of 200 km and a clearly defined period of 62 days. The westward phase speed of the eddies is about 8.6 cm/sec. Both the kinetic and potential energy of the mean flow feed the eddies, but the  $\bar{P}$  to  $P'$  transfer is dominant by about a factor of 10. The Reynolds stresses show that the eddies tend to decelerate the westward flow in which they are imbedded.

In experiment 3 the eddy period is 43-50 days, the half wavelength is 250-350 km in the upper layer, and 250-500 km in the lower layer. The westward phase speed of the eddies is 15-25 cm/sec in the near jet region. The eddy field receives most of its energy by means of barotropic instability in the upper layer circulation, i.e.  $\bar{K}_1$  to  $K_1'$ . The deep eddy field is primarily maintained by work done by the pressure forces at the interface, i.e.  $K_1'$  to  $K_3'$ . The Reynolds stresses tend to intensify the eastward flowing jet representing the Gulf Stream extension.

In experiment 5 the eddy period is about 50 days and the half wavelength is 220 km in the upper layer, 310 km in the lower layer. The mean westward phase speed is approximately 18 cm/sec. The energy pathways are the same as in experiment 3, but the energy transfers are larger. Again the Reynolds stresses tend to accelerate the eastward jet.

4. A linearized stability analysis. Because the solutions in experiments 3 and 5 are quite complex as well as spatially inhomogeneous, local rather than global diagnostic tools are needed. The LSA is one such tool. The basic state for the LSA is assumed to be steady, constant in direction, longstream invariant, and periodic in one direction. This automatically rules out certain classes of instability, most notably the barotropic instability of Rossby waves (Lorenz, 1972). It also eliminates downstream variations whose effects must be important in the finite-amplitude

equilibration of the eddy field (Pedlosky, 1976). The authors substitute the assumed mean and small amplitude perturbation fields into the potential vorticity equations for the model and solve the resulting stability problem numerically using finite difference equations described in the Appendix which are analogous to those used by Holland (1978) for his QG EGCM model. The authors also formulate eddy energy equations for the LSA model. However, the LSA energetics can only predict the relative magnitudes of the energy fluxes, not the absolute magnitudes. The authors note the importance of adequate resolution of the mean jet in the LSA. In some cases degrading the resolution from 20 to 40 km had a marked effect on the results. The authors also mention the problem of resolving possible critical layers (Lin, 1955).

5. A stability analysis interpretation of EGCM results. The authors find that they obtain much more satisfactory results if they average over several realizations of the LSA using representative instantaneous profiles rather than mean profiles for the basic state.

Experiment 1 is the simplest. Only one instability is found, a moderately unstable baroclinic mode in the region of the westward return flow. This is a region of opposing potential vorticity gradients in the upper and lower layers, a necessary condition for baroclinic instability (Pedlosky, 1963). Both the time mean and instantaneous profiles exhibit this instability. Eddies in the lower layer lead those in the upper layer by almost  $90^\circ$ , resulting in a transfer of  $\bar{P}$  to  $P'$  as in a baroclinic instability. The wavelength, period, and westward phase speed predicted by the average for several realizations of the LSA are in excellent agreement with the values from experiment 1. The eigenfunctions also exhibit a N-S elongation of the eddies as observed in experiment 1 and as predicted for a baroclinic instability of a westward zonal current (Robinson and McWilliams, 1974). However, wave radiation into the southern basin observed in the EGCM experiments cannot occur in the LSA.

The LSA predicts not only the direction, but also the relative amplitudes of the energy fluxes to the eddies with surprising accuracy. One exception is the much greater  $\bar{K}_3$  to  $K'_3$  transfer in the EGCM results, evidently a finite amplitude result. The energetics are characteristic of a baroclinic instability with  $\bar{P}$  to  $P'$  dominating  $\bar{K}$  to  $K'$ . The authors also compare the LSA and EGCM latitudinal profiles of  $K'_1$  to  $P'$ ,  $K'_1$  to  $K'_3$ ,

and the Reynolds stresses for the upper and lower layers. The first two are in remarkable structural agreement, but the latter two are not. In both cases the Reynolds stresses tend to retard the westward jet in the upper layer, but the EGCM Reynolds stress profiles tend to be broader, presumably as a result of eddy energy propagation away from the original latitude.

In experiment 3 at least 3 instabilities are periodically or continuously active: a barotropic mode in the central eastward flowing jet, and two baroclinic modes in the westward return flows north and south of it. However, when time averaged profiles were used, the barotropic instability was not detected. The meandering of the current tends to broaden the mean current. Hence, it was necessary to use instantaneous profiles in the LSA's. When this was done, the most unstable mode predicted by the LSA was barotropic and occurred in the eastward current. This mode also exhibited barotropic energy transfer characteristics with  $\bar{K}_1$  to  $K'_1$  and  $K'_1$  to  $K'_3$  as in the EGCM results (the baroclinically unstable case exhibited  $K'_3$  to  $K'_1$ ). However, the LSA statistics for different profiles varied substantially and the means were only fair predictors of the EGCM results. The LSA also detected the weaker baroclinic instability of the westward return currents, which is similar to that in experiment 1. In the EGCM global energetics for experiment 3, the baroclinic instabilities contribute little, because of intermittency and/or slower growth rates. The meridional profiles of the barotropically unstable modes for the energy transfers and the Reynolds stresses discussed for experiment 1 are quite different from the EGCM results except for a peak at the center of the basin for  $K'_1$  to  $P'$  and  $K'_1$  to  $K'_3$ . This situation might be improved by the superposition of several unstable modes. The LSA Reynolds stresses predict a deceleration of the eastward jet and the westward return flow in the upper layer, as expected for a barotropically unstable flow. However, the finite amplitude EGCM results show an acceleration of the eastward jet.

The EGCM results for experiment 5 are similar to those of experiment 3, but are more energetic and even more chaotic. The LSA detects the existence of the basic instabilities when instantaneous meridional profiles are used for the basic state. It also predicts the direction of the dominant  $\bar{K}_1$  to  $K'_1$  and  $K'_1$  to  $K'_3$  energy transfers. However, the authors find little success beyond this for the LSA.

The authors also investigate the stability of the western boundary current and the broad interior Sverdrup return flow. They find no baroclinic instabilities, but do find a barotropic instability near the seaward edge of the western boundary current, but one with a slower growth rate than instabilities found in the zonal currents, and it appears to have been masked by the latter in the EGCM results.

6. Conclusions. (1) The LSA was able to correctly identify regions of instability in the EGCM. (2) The LSA showed some success in predicting the lower order statistical features (wavelength, growth rate, period and phase speed) of the equilibrium eddy fields. (3) The LSA was able to identify some less unstable regions that are masked in the global energetics of the EGCM results. (4) The LSA showed some success at predicting higher order statistics such as the net sign and cross-stream structure of the intra-eddy energy fluxes,  $P'$  to  $K'_1$ ,  $K'_1$  to  $K'_3$ , etc., but was unsuccessful in predicting the Reynolds stresses. (5) The presence of barotropic instability which depends on horizontal shears can be severely underestimated, if mean profiles are used as the basic state. Much greater success was obtained using instantaneous profiles.

The authors plot the results of their stability analyses on a scatter diagram of vertical versus horizontal shear. The instabilities are classified as barotropic, baroclinic, or mixed on the basis of the dominant global energy fluxes. Clearly defined regions are found to exist for each. However, other parameters held invariant here should be important, e.g. Hart (1974) has noted the dependence of the mixed instability problem on the eddy Froude number ( $F_e = f_0^2 L_e^2 (H_1 + H_3) / g' H_1 H_3$ , where  $L_e$  is the eddy length scale), and on the layer depth ratio ( $\delta = H_1 / H_3$ ) in a two-layer QG model on an f-plane. For the parameters used in this study, the threshold value for baroclinic instability is  $\Delta u \approx 5$  cm/sec across the thermocline, that for barotropic instability is a horizontal shear of about  $3 \times 10^{-6}$  sec<sup>-1</sup>. Persistent shears of this order are probably not found in the mid-ocean. The results reported here support the contention that regions of intense currents such as the Gulf Stream, and not the mid-ocean, are the primary sites of eddy generation and growth.

## REFERENCES

- Hart, J. E., 1974: On the mixed stability problem for quasi-geostrophic ocean currents. J. Phys. Oceanogr., 4, 349-356.
- Holland, W. R., 1978: The role of mesoscale eddies in the general circulation of the ocean - Numerical experiments using wind-driven quasi-geostrophic model. J. Phys. Oceanogr., 8, 363-392.
- Lin, C. C., 1955: The Theory of Hydrodynamic Stability, Cambridge University Press, 155 pp.
- Lorenz, E. N., 1972: Barotropic instability of Rossby wave motion. J. Atmos. Sci., 29, 258-264.
- Pedlosky, J., 1963: Baroclinic instability in two layer systems. Tellus, 15, 20-25.
- Pedlosky, J., 1976: Finite-amplitude baroclinic disturbances in downstream varying currents. J. Phys. Oceanogr., 6, 335-344.
- Robinson, A. R. and J. C. McWilliams, 1974: The baroclinic instability of the upper ocean. J. Phys. Oceanogr., 4, 281-294.

18 Jun 1981

SUMMARY #10 by Harley E. Hurlburt

Hart, J. E., 1974: On the mixed stability problem for quasi-geostrophic ocean currents. J. Phys. Oceanogr., 4, 349-356.

1. Introduction. This study was motivated by the desire to understand under what conditions atmospheric and oceanic eddies might be stable. Long-lived mesoscale ring currents in the ocean often take the form of localized solid body rotation with shear zones outside some characteristic distance,  $L$ , in which the azimuthal velocity is brought to zero. However, these ring currents do not satisfy any known sufficient condition for stability of quasi-geostrophic flow in the upper layer of a two-layer, flat-bottom, inviscid ocean on a  $\beta$ -plane. This study uses such a model to study a mixed barotropic/baroclinic linear stability problem for currents resembling the rings. It concentrates on the possible influences of rotation and stratification as measured by the internal Froude number,  $F = f^2 L^2 / g' H_1$ , and the layer thickness ratio,  $\delta = H_1 / H_2$ , where  $f$  is the Coriolis parameter,  $g'$  is the reduced gravity  $g \Delta \rho / \rho$ , and  $H_1$  and  $H_2$  are thicknesses of the upper and lower layers. The possibly important effects of  $\beta$  and topography are ignored.

The critical Froude number for baroclinic instability of a simple uniform channel flow  $U_1 = \text{constant}$ ,  $U_2 = 0$  is simply  $F_C \approx \frac{1}{2} \pi^2 / \delta^{1/2}$ . However, Lipps (1963) has shown that if one makes  $F$  large enough in a one-layer model, the potential vorticity gradient is positive or negative definite and the system becomes barotropically stabilized. Putting these two results together one sees that as  $\delta$  gets small the upper layer behaves more and more like a divergent one-layer fluid and  $F$  can then be made large enough to stabilize the shear zone of the eddy without getting baroclinic instability. This conjecture is tested here, a conjecture which in part depends on the assumption that there be no mixed modes of instability in the proposed stable transition zone between the regions of barotropic and baroclinic instability.

2. The model is two-layer, flat-bottom,  $f$ -plane, inviscid, and quasi-geostrophic. The basic flow is confined to the upper layer and for convenience it is also a rectilinear channel flow. Hart asserts that only slight quantitative differences should result if the basic flow were axisymmetric. The cross-stream structure of the basic state is uniform flow for  $0 \leq x \leq L$  to model the solid body rotation part of a

circular eddy. For  $x > L$  the flow decays exponentially to zero to model the shear zone. Linear stability is examined in equations expressing conservation of perturbation potential vorticity (Pedlosky, 1964). The channel width is chosen great enough to have minimal effect on the results.

The model satisfies the necessary condition for instability that  $v_1(-v_{1xx} + Fv_1) > 0$  somewhere (Pedlosky, 1964) as do observed ring currents. However, this does not mean that instability will actually occur. The upper layer potential vorticity gradient is positive definite if  $F > \lambda^2$  where  $\lambda$  is the exponential decay constant in the shear zone of the basic state. If the addition of baroclinic processes does not alter the stability properties of the divergent one-layer models, then instabilities should not be generated by kinetic energy transport from the basic flow when  $F > \lambda^2$ . Since good initial guesses were not available for the eigenvalues, the problem was converted to a matrix eigenvalue problem to facilitate the solution.

3. Results. The basic results of the stability analysis are summarized in a stability regime diagram for  $F$  vs.  $\delta$  shown in Fig. 1. A stable regime is

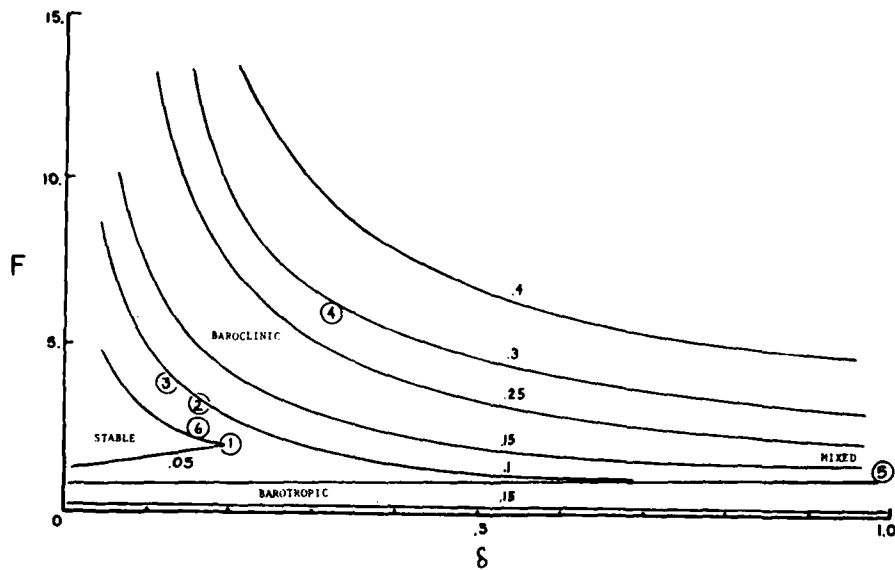


Fig. 1. Contours of nondimensional growth rates in  $F$ ,  $\delta$  space for  $\lambda = 2$ ,  $A = 4$ . Also indicated by circled numbers are the parametric positions of observed eddies.

found for small  $\delta$  and moderate  $F$ . Regimes with baroclinic, barotropic, and mixed instability are also found. Tests with two different values of  $\lambda$  showed that increasing the shear increased the tendency for barotropic instability. Hart speculates that the region of stability would be slightly larger for circular flows. In sample calculations of the flow field, perturbation flow was mostly confined to the upper layer in the barotropically unstable case. In the baroclinically unstable case it was strong in both layers and exhibited a phase shift between the layers. In both cases the perturbation was strongest at the inside edge of the shear zone near  $X = L$ .

4. Conclusions. Some observations of oceanic eddies have allowed estimates of  $\delta$  and  $F$ . Results for several observed eddies are plotted on Fig. 1 as circled numbers. Their behavior tends to support the results of the stability analysis. Eddy ④ was situated over a seamount and eddy ⑤ was unstable. The others appear to be in regimes of weak instability on the stability diagram. However, possibly stabilizing influences of topography, friction, and flow in the lower layer (to change the vertical shear) have not been included. The effect of  $\beta$  on the stability problem can be estimated from

$$\frac{H_1}{R \frac{\partial h}{\partial y}}$$

where  $R$  is the radius of the earth and  $\partial h / \partial y$  is the interface slope inside the eddy. This ratio is  $\sim 1/20$ . A rough estimate of the necessary conditions for stability are  $F > \lambda^2$  and  $\delta \lesssim F^{-1.4}$  (when  $\lambda \geq 2$ ).

#### REFERENCES

Lipps, F., 1963: The stability of jets in a divergent barotropic flow. J. Atmos. Sci., 20, 120-129.

Pedlosky, J., 1964: The stability of currents in the atmosphere and ocean: Part I. J. Atmos. Sci., 21, 201-219.

## SUMMARY #11 by Harley E. Hurlburt

Semtner, A. J., Jr., and W. R. Holland, 1978: Intercomparison of quasi-geostrophic simulations of the western North Atlantic circulation with primitive equation results. J. Phys. Oceanogr., 8, 735-754.

1. Introduction. The purpose of this paper is to compare two eddy-resolving numerical ocean models (EGCM's) of vastly different complexity and computational requirements, namely the two-layer quasi-geostrophic (QG) model of Holland (1978) and the five-level primitive equation (PE) model of Semtner and Mintz (1977). The simulation is for a wind-driven multi-gyre ocean including the effects of bottom topography and thermal forcing. The first EGCM study used a two-layer PE model (Holland and Lin, 1975a,b). Since then Haidvogel (1976), Holland (1978), and McWilliams, et al (1978) have used QG models in EGCM studies, while Han (1975), Robinson, et al (1977) and Semtner and Mintz (1977) have used multi-level PE models. Both approaches have shown a number of common features, including unstable eastward free jets. The mesoscale eddies which arise spontaneously transfer energy downward via the vertical pressure-work term. However, some significant differences are also apparent. The single gyre study of Holland and Lin (1975a) and Holland (1978) showed dominant baroclinic instability, but the single gyre experiment of Robinson, et al showed barotropic instability dominant. The simulations of Han (1975) and Semtner and Mintz (1977) showed weak baroclinic instability for the North Equatorial flow, where the simple QG models show none. Are the differences due to parametric differences or to model deficiencies, such as an over-extension of the QG assumptions and neglect of thermal forcing and bottom topography in the simple models, or to the inclusion of excessive heat diffusion and the inability to make sufficiently long-term integrations in the more complicated PE models? Clearly a comparison of the two types of models for this physical problem is needed.

To save computer time the QG model is compared with an existing PE experiment, that of Semtner and Mintz (1977) (S&M). That experiment includes a free jet, strong eddies, thermal forcing, biharmonic friction, and a continental slope parallel to one boundary. Once the QG-PE comparison is completed, additional QG results are presented to examine the effects on

the general circulation of thermal forcing, bottom topography, upper layer depth, and the addition of a third layer.

2. Formulation of the quasi-geostrophic model. The two-layer QG model is that of Holland (1978) with the addition of bottom topography and thermal forcing (see Summary #4). It consists of vorticity equations for the two model layers and a thermodynamic equation at their interface. It uses highly scale selective biharmonic lateral friction. The bottom topography is included in linearized form as a lower layer vortex stretching term. It is also included in the linear bottom friction term (S&M use quadratic bottom friction). The thermal forcing,  $Q$ , appears as a source term in the thermodynamic equation. The QG experiment is designed to match the PE experiment of S&M within the context of its simplicity. For the purpose of the comparison large amplitude continental shelf topography is allowed in the QG experiment even though this violates the QG approximation. Unlike the S&M simulation, the QG model neglects lateral heat diffusion, but uses double the coefficient for biharmonic lateral diffusion of momentum. Both models use free slip boundary conditions and a horizontal grid increment of 37 km. In the QG model the time step  $\Delta t = 6$  hrs., but in the PE model it is only 40 min. due to the presence of internal gravity waves. Overall the two-layer QG model is 40 times faster than the 5-level PE.

3. The state of statistical equilibrium is reached after two to three years in the QG model, after much longer in the 5-level PE model. In the QG model the thermal input is about 35% of the wind input and the dissipation by lateral and bottom friction are about the same. Both PE and QG experiments exhibit similar patterns, including an unstable mid-latitude free jet. The associated eddies have a wavelength  $\sim 600$  km and comparable westward propagation speeds. Both models exhibit eddies in the SW basin. The time averaged circulations and mean eddy energy distributions of the two simulations are also similar both near the surface and in the deep water. Due to the expected influence of topography and thermal forcing on the lower layer flow, the lower layer agreement is especially notable. Both models predict a time-averaged transport of 240 Sv for the Gulf Stream.

4. Energetics. The authors present the formulation of the eddy-mean energetics for the two-layer QG model, which can be represented in the form of a 6-box diagram. The upper and lower layer kinetic energies can

be combined to produce 4-box energy diagrams like those used by S&M. This was done for the basin averaged comparisons of the QG and PE simulations. With  $H_1 = 500$  m, no lateral heat diffusion and similar energy inputs to the models, the energy levels in the QG model were about 35% higher. The eddy-mean energy transfers are much different. The PE model exhibits a very dominant baroclinic instability ( $\bar{P}$  to  $P' \gg \bar{K}$  to  $K'$ ), while the QG model exhibits mixed instability ( $\bar{P}$  to  $P' \approx \bar{K}$  to  $K'$ ), where  $P$  is potential energy,  $K$  is kinetic energy, an overbar denotes the mean flow component, a prime the eddy flow component.

Since the free jet in the PE model is more strongly surface trapped than in the QG model with  $H_1 = 500$  m, the authors repeated the QG experiment with  $H_1 = 200$  m and with (unimportant) heat diffusion added. This time the energy levels (except for  $P$ ) and energy transfers in the QG and PE models were in good agreement. Plots of  $P'$  to  $K'$  vs. latitude showed weak baroclinic instability in the north equatorial current in the PE and both QG experiments. The dominant instability was in the vicinity of the free jet. It was predominantly baroclinic in the PE simulation and in the QG simulation with  $H_1 = 200$  m, but predominantly barotropic in the QG simulation with  $H_1 = 500$  m.

5. Some parameter variations were made using the more efficient QG model, since its validity had been bolstered by comparison with the PE model. In all, results of eight QG experiments are presented in which the parameters varied are the number of layers(2 or 3), upper layer thickness ( $H_1 = 200$  m or 500 m), thermal forcing (present or absent), continental slope topography (present or absent), and heat diffusion (present or absent). The continental-slope topography substantially strengthens the upper layer mean jet for a considerable distance off shore. The thermal forcing does the same, but only to a slight extent. The continental slope substantially modifies the deep mean flow, the thermal forcing to a much lesser extent. The experiment with both thermal forcing and topography is in best agreement with the PE results. The 6-box energy diagrams show that neither topography nor thermal forcing had a major effect on the global energetics. The topography did tend to increase the potential energy and  $\bar{K}_1$  (upper layer), while reducing  $K'_3$  (lower layer). All four experiments with  $H_1 = 500$  m

exhibit a mixed instability with both  $\bar{K}$  and  $K'$  transported downward. Most of the frictional loss is from the eddies.

A second group of experiments has  $H_1 = 200$  m. One pair of these has three layers with or without topography, the other has lateral heat diffusion with or without topography. All four include thermal forcing. In the 2-layer cases  $g' = .02$  m/sec<sup>2</sup>. In the three-layer experiments  $g' = .013$  m/sec<sup>2</sup> at the upper interface and .007 m/sec<sup>2</sup> at the lower interface at 600 m depth. Thermal forcing is included only at the upper interface. With  $H_1 = 200$  m, the upper layer flows are somewhat stronger. However, the upper and lower layer mean flow patterns are not altered much by the addition of a third layer. The two-layer case with  $H_1 = 200$  m exhibits the greatest intensification of the upper layer free jet due to topography. When the thermal forcing is applied at the shallower 200 m depth, its influence on the deep flow is noticeably decreased.

In the three-layer experiments the global energetics are about the same with or without topography. The most notable consequence of changing  $H_1$  from 500 m to 200 m is the dominant baroclinic instability at the 200 m interface in all four experiments with  $H_1 = 200$  m. The authors contend this is augmented by the thermal forcing. In the three-layer experiments  $K'_3$  to  $K'_1$  and  $K'_3$  to  $K'_5$  (third layer) conversions also occur. In the two layer experiments with  $H_1 = 200$  m  $K'_1$  to  $K'_3$  occurs in the flat bottom case, but weak  $K'_3$  to  $K'_1$  occurs in the case with a continental slope. The latter case is <sup>the</sup> most baroclinically unstable of all the QG experiments. A plot of  $P'$  to  $K'$  vs. latitude shows that the mid-latitude free jet emanating from the region of the continental shelf is the feature which is baroclinically destabilized by the bottom topography. It also shows that the baroclinic instability of the mid-latitude free jet is concentrated at the upper interface, whereas that of the north equatorial current is more evenly distributed between the two interfaces.

Typically, the mean available potential energy (APE) of the two-layer experiments is about twice as large as the PE value. However, the PE and three-layer QG models have APE's which are in much closer agreement. Although the two-layer model correctly predicts the amount of vertical shear (proportional to  $\psi_1 - \psi_3$ , where  $\psi_i$  is the streamfunction

in layer i) between the surface and deep layers, it exaggerates the APE (proportional to  $(\psi_1 - \psi_3)^2$ ), because it is concentrated at a single interface. In the three layer case, a correct magnitude of the vertical shear  $(\psi_1 - \psi_5)$  implies a smaller value of APE (proportional to  $(\psi_1 - \psi_3)^2 + (\psi_3 - \psi_5)^2$ ), where i = 1, 3, 5 are the indexes for the top, second, and third layers.

6. Discussion. These comparisons indicate that QG models reproduce most of the basic dynamical features of a mid-latitude PE model, despite strong non-linearity and mesoscale variability, and the inclusion of thermal forcing and bottom topography. Both the continental slope topography and the thermal forcing significantly affect the QG results, and adding both improves the QG-PE agreement. It appears that the linearized treatment of the large amplitude continental slope and the application of the thermal forcing at the QG interface adequately reproduce features of the nonlinear PE model. Because of its efficiency, the QG model is the clear choice for mid-latitude EGCM parametric studies. The authors also mention some limitations of QG models and concede that the optimal modeling approach is problem dependent.

## REFERENCES

- Haidvogel, D. B., 1976: The sensitivity and predictability of mesoscale eddies in an idealized ocean model. Ph.D. thesis, Massachusetts Institute of Technology, 250 pp.
- Han, Y.-J., 1975: Numerical simulation of mesoscale ocean eddies. Ph.D. thesis, University of California at Los Angeles, 154 pp.
- Holland, W. R., 1978: The role of mesoscale eddies in the general circulation of the ocean - Numerical experiments using a wind-driven quasi-geostrophic model. J. Phys. Oceanogr., 8, 363-392.
- Holland, W. R., and L. B. Lin, 1975a: On the generation of mesoscale eddies and their contribution to the oceanic general circulation. I. A preliminary numerical experiment. J. Phys. Oceanogr., 5, 642-657.
- Holland, W. R. and L. B. Lin, 1975b: On the generation of mesoscale eddies and their contribution to the oceanic general circulation. II. A parameter study. J. Phys. Oceanogr., 5, 658-669.
- McWilliams, J. C., W. R. Holland, and J. H. S. Chow, 1978: A description of numerical Antarctic Circumpolar Currents. Dyn. Atmos. Oceans, 2, 213-291.
- Robinson, A. R., D. E. Harrison, Y. Mintz, and A. J. Semtner, Jr., 1977: Eddies and the general circulation of an idealized oceanic gyre: A wind and thermally driven primitive-equation numerical experiment. J. Phys. Oceanogr., 7, 182-207.
- Semtner, A. J., and Y. Mintz, 1977: Numerical simulation of the Gulf Stream and mid-ocean eddies. J. Phys. Oceanogr., 7, 208-230.

## SUMMARY #12 by Harley E. Hurlburt

McWilliams, J. C. and G. R. Flierl, 1979: On the evolution of isolated, nonlinear vortices. J. Phys. Oceanogr., 9, 1155-1182.

1. Introduction. This paper is an excellent study of the evolution of isolated, nonlinear vortices using a numerical two-layer, quasi-geostrophic (QG), adiabatic model on a  $\beta$ -plane. It is motivated by the observation that the Gulf Stream and other major currents shed strong eddies that become isolated from the stream and other eddies of comparable strength. The eddies are highly baroclinic and strongly nonlinear with a typical beta Rossby number,  $Q = V_0/\beta L^2 \approx 13$ , where  $V_0$  is a typical particle speed for a Gulf Stream ring ( $\sim .8$  m/s),  $\beta$  is the northward gradient of the Coriolis parameter ( $1.7 \times 10^{-11}$  m $^{-1}$  s $^{-1}$  at  $40^\circ$  latitude), and  $L$  is a typical pressure e-folding radius of a ring ( $\sim 60$  km). The rings decay slowly. Cheney and Richardson (1974) observed one where the transport decreased  $< 25\%$  in eight months. The cyclonic Gulf Stream rings typically move to the SW at  $\sim 3$  cm/s in the direction of the flow for the mean thermocline circulation. The vertical structure of the rings appears to vary from purely baroclinic (zero total transport) to compensated (zero deep flow) to lower layer flow weakly in phase with the upper layer.

This study concentrates on the influence of nonlinearity on the unforced evolution of an initially axially symmetric Gaussian vortex in a doubly periodic otherwise quiescent ocean. With  $\beta = 0$ , an inviscid, stationary, axially symmetric vortex is a steady, though not necessarily stable solution to the model. With the addition of lateral friction, the vortex remains stationary, but its radial profile changes and its amplitude decreases with time without change in vertical structure. With  $\beta$  present a small amplitude, axially symmetric, frictionless vortex propagates west and rapidly disperses and decreases in amplitude, unless its radius is large compared to the radius of deformation appropriate to its vertical structure (Flierl, 1977). This paper focuses on the combined effects of  $\beta \neq 0$  (essential to vortex propagation) and nonlinearity (which significantly alters the rates of propagation, decay, and dispersion, and allows for strong interactions between different vertical modes). Systematic studies are made of the consequences of varying the frictional coefficient, the vortex amplitude and radius, the degree of nonlinear coupling between the two vertical modes, and on the initial vertical structure of the vortex.

2. Mathematical formulation. The two vertical mode QG model is physically equivalent to either a two-layer or two-level model. The pressures in the upper and lower layers,  $p_1$  and  $p_2$  are related to the pressure for the barotropic and baroclinic modes ( $p_T$  and  $p_C$ ) by

$$p_1 = p_T + \delta^{-\frac{1}{2}} p_C$$

$$p_2 = p_T + \delta^{\frac{1}{2}} p_C$$

where  $\delta = H_1/H_2$  is the undisturbed layer thickness ratio (see Flierl, 1978). The parameter  $v$  is the fraction of the initial vortex components which is barotropic. For a compensated vortex (no lower layer flow),  $v = \delta^{\frac{1}{2}}$ . The QG potential vorticity equations are presented in modal form and have the following nondimensional parameters:

$$Q = V_0/\beta L^2 \quad \gamma = L/R$$

$$\hat{Q} = \frac{1 - \delta}{\delta^{\frac{1}{2}}} Q \quad K^* = K/\beta L^5$$

where  $R = (g' H_1 H_2 / (H_1 + H_2))^{\frac{1}{2}} / f_0$  is the internal radius of deformation,  $g'$  is the reduced gravity and  $f_0$  is the reference value of the Coriolis parameter.  $K$  is the coefficient of a highly scale selective biharmonic momentum diffusion which assures computational stability, without much damping at larger scales, by damping enstrophy which can accumulate at the smallest resolved scales due to nonlinear transfers between scales. In many of the simulations in this paper, friction also plays a physical role in regulating the rate of vortex decay. The QG model solutions are symmetric in the sense that a high-pressure vortex can be reinterpreted as a low-pressure vortex by reversing north and south.

For application of the model results to Gulf Stream rings the authors recommend the following parameters:  $H_1 = 700$  m,  $H_2 = 4300$  m,  $L = 60$  km,  $R = 45$  km,  $f_0 = 9 \times 10^{-5}$  sec $^{-1}$ ,  $\beta = 1.7 \times 10^{-11}$  m $^{-1}$  s $^{-1}$ ,  $V_0 = .8$  m/s, and  $g' = .027$  m/s $^2$ . These imply the following values for the dimensionless parameters:  $Q = 13$ ,  $\hat{Q} = 27$ ,  $\delta = .16$ , and  $\gamma^2 = 1.8$ .

3. A single mode vortex is studied using a single mode or equivalent barotropic model, which the authors choose to write in terms of the internal mode, so that  $Q$  drops from the problem. The standard parameters the authors use for the equivalent barotropic model are  $\hat{Q} = 10$ ,  $\gamma^2 = 2$ , and  $K^* = 5 \times 10^{-4}$ . These imply a strongly nonlinear, slowly decaying eddy with an e-folding radius

$L = \sqrt{2} R$ , the radius of deformation. The value of  $\gamma^2$  is appropriate for a reduced gravity model of a mesoscale eddy. In this case an anticyclonic vortex moves WSW at 2.8 cm/sec and leaves behind a weak Rossby wave wake with a characteristic herringbone pattern (see Rhines, 1977, Fig. 11 or Summary #6, Section 8H). After approximately six months, it has also developed a weak wavenumber 1 axial asymmetry, where nondimensional time ( $t \sim 17$ ) has been scaled by  $\rho L$ . For  $K^* \ll 1$ , the movement of the eddies is insensitive to  $K^*$ , but it is sensitive to  $\hat{Q}$  and  $\gamma^2$ , as shown in Fig. 1,

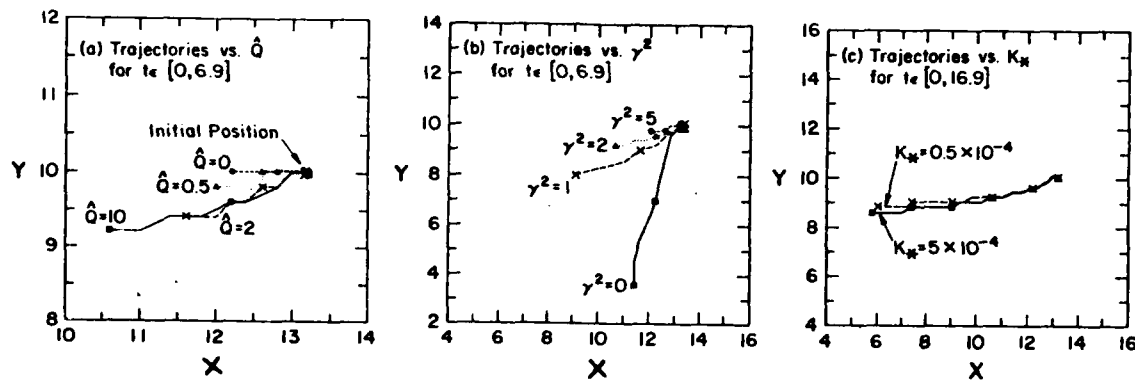


Fig. 1. Trajectories for pressure maxima from numerical solutions for the single-mode vortex initial value problem: (a) trajectories vs.  $\hat{Q}$  for  $0 \leq t \leq 6.9$ , (b) trajectories vs.  $\gamma^2$  for  $0 \leq t \leq 6.9$ , and (c) trajectories vs.  $K^*$  for  $0 \leq t \leq 16.9$ . Except for the parameter varied on each panel, the standard parameters are used. The dots indicate position every  $\Delta t = 3.45$ .

which is based on eight numerical experiments. As  $\gamma$  is decreased, the speed of translation increases and the direction becomes more southerly. For  $\gamma = 0$  (the barotropic case) and  $\hat{Q} = 10$ , it is SSW.

As  $\hat{Q}$  is increased the speed of translation increases, and a southward component develops which appears to reach an asymptotic value as  $\hat{Q}$  is increased. For  $\hat{Q} = 0$ , the propagation is due west and accelerates until it reaches the non-dispersive linear wave speed,  $dx_c/dt = -1/\gamma^2$ , where the subscript, c, indicates

the pressure center of the vortex. For  $\hat{Q} > 0$  and  $\gamma \gtrsim 1$ , the isolated eddies also accelerate toward  $dx_c/dt = -1/\gamma^2$ , but more rapidly. The maximum westward velocity occurs when  $\gamma^2 \approx 1$ . The meridional group velocity,  $-dy_c/dt$ , increases from 0 for  $\hat{Q} = 0$  to an asymptotic value of  $\frac{1}{4}\gamma^2$  as  $\hat{Q}$  increases, except when  $\gamma^2 \ll 1$ . As  $t \rightarrow \infty$ ,  $-dy_c/dt$  decreases to zero. When  $\gamma^2 < 1$ , it is actually possible to have  $-dy_c/dt > -dx_c/dt$  as seen in Fig. 1b. For  $\gamma^2 \gtrsim 1$ , both  $dx_c/dt$  and  $dy_c/dt$  are close to the bounding values from linear theory. In contrast the center of mass of the vortex system always moves due west at the maximum linear wave speed  $1/\gamma^2$ . This discrepancy between the movement of the center of mass and the pressure center is due to dispersion, the meridional motion to nonlinear asymmetric dispersion, subjects the authors discuss in some detail. Dispersion decreases as either  $\gamma^2$  or the nonlinearity  $\hat{Q}$  increases. For a linear dispersive Rossby wave the frequency  $\omega$  is given by

$$\omega = \frac{-k}{k^2 + l^2 + \gamma^2}$$

where  $k$  and  $l$  are zonal and meridional wavenumbers. In this case the meridional group velocity can range between  $-\frac{1}{4}\gamma^2$  and  $\frac{1}{4}\gamma^2$ . The authors discuss how these values limit the meridional propagation speed in the non-linear case. An isolated high pressure vortex has leading and trailing dispersion centers with secondary circulations that both act to advect the main vortex southward. A possible interpretation of the meridional motion of the vortex is that it reflects a tendency to move from an initial latitude,  $y_0$ , to the rest latitude,  $y_r = y_0 - \hat{Q}(\gamma^2 + 4)$ , where a fluid particle retains its initial value of potential vorticity but with no motion. This certainly does not happen completely.

The authors also investigate influences on vortex evolution by means of an asymptotic expansion as  $t \rightarrow 0$ .  $O(t)$  nonlinear effects can be neglected due to the axial symmetry near  $t = 0$ . The  $O(t)$  tendency due to  $\beta$  is primarily westward propagation, that due to friction is radial diffusion with decay of the central amplitude. By comparing the shape of the  $O(t)$   $\beta$  tendency and the shape of the vortex velocity profile, it is possible to determine the extent to which the tendency represents pure propagation. Any excessive tendency represents dispersion. When the westward  $O(t)$   $\beta$  tendency exceeds that for pure propagation, there is a tendency for a positive (negative) center to develop ahead of (behind) the main vortex. The central negative value of the  $O(t^2)$   $\beta$  tendency represents a combination of propagation and decay of the central amplitude of the vortex, while its leading and trailing positive centers

represent further dispersion and westward propagation. Nonlinear self-interactions of the initially propagating and dispersing vortex are dominant at  $O(t^2)$  and  $O(t^3)$ . At  $O(t^2)$  nonlinearity provides a tendency for southward propagation, at  $O(t^3)$  a tendency for augmented westward propagation. Since the nonlinear tendencies have slightly smaller scales than the main vortex, they provide little dispersion, and at  $O(t^3)$  there is even a weak tendency to cancel the dispersion of the  $O(t)\beta$  tendency. Because the single-mode vortex retains much of its initial character, a qualitative application of the small time tendencies to larger times is possible. This is illustrated by drawing maps of the potential vorticity equation terms at finite time. The  $\beta$  term represents a westward propagation and dispersion tendency, the frictional term decay and flattening of the vortex, and the nonlinear term southwestward propagation.

The last topic in this section is the decay of the central pressure maximum. The authors show that nonlinearity can substantially reduce the rate of vortex decay due to linear wave dispersion. Increasing  $\gamma^2$  can also greatly reduce the rate of decay. Even with the very small amount of friction used in these numerical experiments, the decay rate is governed mostly by friction for large values of  $\gamma^2$  and  $\hat{Q}$ .

4. A baroclinic vortex in a two-mode model. The authors first consider an initially purely baroclinic vortex ( $v = 0$ ) in a two-mode model. The standard parameters for the single mode model plus  $\delta = .16$  are used. This implies  $Q = 4.76$ . Initially, the internal mode develops much as in the single mode solution with similar southwestward propagation and a similar dispersion pattern. The barotropic mode develops a counter-rotating vortex pair. At an intermediate time of  $t = 9.2$  or 104 days, the rate of intensification of the barotropic vortex pair greatly slows and the westward motion of the baroclinic vortex is arrested. Later, the baroclinic vortex returns to southwestward propagation, while the barotropic centers separate and radiate Rossby waves, and eventually become highly meridionally asymmetric. The baroclinic field retains the character of an isolated vortex, while the barotropic field tends toward a uniform eddy field.

Initially, the baroclinic center lies between the two barotropic ones, but soon shifts southward over the barotropic eddy with like rotation, as all three centers begin to move eastward. Once there is sufficient southward displacement of the anticyclonic centers, separating them from the cyclonic barotropic vortex, they move southwestward, while the cyclonic center moves

northwestward. The latter movements can be anticipated from the study of the single mode vortex. For  $t \leq 6$  there is a strong conversion of energy from the baroclinic to barotropic mode; later this becomes much weaker. The amplitude decay rate in the two-mode model is initially much greater and later slightly greater than in the single mode model. The baroclinic vortex trajectory of the two-mode model differs from the WSW trajectory of the one-mode model by exhibiting an S-shape (WSW-S-E-S-SW) up to  $t \sim 15$ , and a SW trajectory after that.

Two more initially baroclinic numerical experiments were performed, one with  $\gamma^2 = 5$ , the other was less nonlinear with  $\hat{Q} = 2$ . With  $\hat{Q} = 2$  the baroclinic vortex trajectory was SW for all time. This case exhibits slower modal energy conversion and more vortex dispersion, than when  $\hat{Q} = 10$ . For a larger baroclinic vortex  $\gamma^2 = 5$ , the initially westward propagation is arrested and a persistent southeastward trajectory develops for an intermediate time scale. The baroclinic amplitude decay is slower than when  $\gamma^2 = 2$ , as was the case for the single mode vortex.

Two of the most prominent differences between these two-mode and one-mode solutions are the spinup of the barotropic vortex pair and the tendency for eastward propagation of the baroclinic vortex due to modal coupling. Both of these features can be seen in the small  $t$  asymptotic solutions. Each of the tendencies already discussed for the single mode solution is also applicable to the two-mode case with  $v = 0$ . The leading order barotropic term occurs at  $O(t^2)$  due primarily to baroclinic advection of baroclinic vorticity associated with the  $O(t)$  linear wave dispersion. Its structure provides the tendency for the development of a meridionally antisymmetric vortex pair. The dominant barotropic term at  $O(t^3)$  tends to give a clockwise rotation to the latter. The leading order barotropic back interaction on the baroclinic vortex is at  $O(t^3)$  and provides a tendency for eastward propagation. The authors also use results from moment equations to discuss how the relative locations of the baroclinic and barotropic vortices affects the direction and speed of propagation.

When propagating with an eastward component, the baroclinic vortex approaches a nontransient solitary eddy solution known as a vortical modon (Flierl, et al, 1980). This solution consists of an eastward propagating, barotropic, counter-rotating vortex pair, with the anticyclonic member to the south. This is accompanied by a passive axisymmetric baroclinic

mode vortex of arbitrary amplitude, although the modon becomes unstable when the baroclinic streamfunction amplitude is at least comparable to that of the barotropic mode. The eastward propagation depends on the amplitude and separation of the barotropic vortices. The authors verify that at least one of their solutions temporarily fits this model. For later times the standard experiment and many others approach a compensated flow, i.e., with no flow in the lower layer (also see Mied and Lindemann, 1979). In this case the ratio of the barotropic and baroclinic streamfunction amplitude is approximately,  $v = \delta^{\frac{1}{2}}$ .

5. Mixed mode vortices with both modes non zero ( $v \neq 0$ ). In this section special attention is given to the tendency toward compensated flow. The first experiment with initially mixed modes uses a compensated vortex as an initial state, i.e.,  $v = \delta^{\frac{1}{2}} = .4$ . The vortex modes propagate southwestward together and remain nearly compensated, although there is more dispersion of the barotropic mode. Continuing compensation despite barotropic dispersion is handled partly by a transfer of energy from the baroclinic to the barotropic mode through nonlinear coupling, and partly by shrinking of the barotropic vortex diameter.

Increasing  $v$  from .4 to 1 has little effect. Unlike the case with  $v = 0$ , there is uniform southwestward propagation. The speed of propagation is 40% faster than in the single mode case, and the direction is SW rather than WSW. As  $v$  is increased, the initial amplitude decay rate of the baroclinic vortex is decreased, since there is less need for transfer to the barotropic mode to maintain compensation. At large times the decay rate is nearly the same for initial  $v = 0, .4, 1$ , since all these cases approach a state of deep compensation. The authors discuss the mixed mode trajectories in terms of the small  $t$  asymptotic analysis. The two modes would not propagate together, if propagation were based entirely on the two  $O(t)$  linear  $\beta$  tendencies. Inclusion of the nonlinear tendencies is essential for this. In the compensated vortex case, the authors find southward and westward, but no dominant eastward propagation tendencies.

The authors found that all six of their two-mode experiments eventually reached a compensated state with  $v = \delta^{\frac{1}{2}}$ . Even a case with initial  $v = -.4$ , which exhibited a period of eastward, modon-like propagation, eventually reached a compensated state after  $t \sim 45$ . Thus, the authors investigate both the tendency for persistence of a compensated state and the manner in which that state is reached. For small  $\mu = Q\gamma^2\delta^{\frac{1}{2}}$  (no

effective nonlinear coupling of the two layers), they conclude that since barotropic Rossby waves are highly dispersive, it is unlikely that the lower layer streamfunction amplitude will efficiently increase at any point in the fluid, while the upper layer propagates as a single mode vortex.

For both small and large  $\mu$  and an initially compensated vortex, the authors find a southwestward propagating vortex in the upper layer and a wave dispersion field in the lower layer. However, the direction of the upper layer vortex propagation changes from WSW for small  $\mu$  to more southward for larger  $\mu$ . No vortex stands out in the lower layer for small or large  $\mu$ . Hence, intensification of a lower-layer vortex must be inhibited by the nonlinear terms coupling the two layers.

The authors explain the compensation persistence in terms of the dispersion of lower layer Rossby waves forced by the thermocline interfacial deformation by the upper layer vortex. The approximate dynamical separation of the two layers is a consequence of the thin upper layer and the relative amplitude of the solutions in the two layers. When the two modes are not compensating initially, they will become compensating when the barotropic amplitude is approximately large enough to be compensating. Then the baroclinic vortex center will shift over the barotropic vortex center of like sign by the vortical modon instability mechanism. For an initial excess of barotropic vortex component, it appears that barotropic wave dispersion will efficiently erode the barotropic vortex component until its amplitude is approximately compensating. It does not decrease due to frictional decay or due to nonlinear transfer to the baroclinic vortex.

6. Summary and comparison with other solutions. The baroclinic vortex propagation rate can have a large meridional component due to both baroclinic nonlinear self-interactions and baroclinic-barotropic modal coupling. The westward linear propagation tendency due to  $\beta$  is enhanced by the former process and can be either enhanced or opposed by the latter, depending on the initial conditions. For large  $Q$ ,  $\gamma$ , and small  $\delta$ , there is a general tendency for any vortex with a significant baroclinic initial component to approach a state of deep compensation with little lower layer expression of the main vortex, but with an energetic field of barotropic eddies.

The results in this paper suggest that rings generated by the Gulf Stream should return to it, since cyclonic (anticyclonic) rings with a northward (southward) propagation component form on the south (north) side of the stream. In most cases rings should also propagate westward faster than predicted by linear theory. The results also suggest that rings may be a significant source of other types of eddy energy through nonlinear transfers to the more dispersive barotropic mode.

#### REFERENCES

- Cheney, R. and P. Richardson, 1974: Observed decay of a cyclonic Gulf Stream ring. Tech. Rep. 74-2, University of Rhode Island, 137 pp.
- Flierl, G. R., 1977: The application of linear quasi-geostrophic dynamics to Gulf Stream rings. J. Phys. Oceanogr., 7, 365-379.
- Flierl, G. R., 1978: Models of vertical structure and the calibration of two-layer models. Dyn. Atmos. Oceans, 2, 341-381.
- Flierl, G. R., V. D. Larichev, J. C. McWilliams and G. M. Reznik, 1980: The dynamics of baroclinic and barotropic solitary eddies. Dyn. Atmos. Oceans, 5, 1-41.
- Rhines, P. B., 1977: The dynamics of unsteady currents. The Sea, Vol. 6, Wiley Interscience, 189-318.

24 June 1981

SUMMARY #13 by Harley E. Hurlburt

Ikeda, M., 1981: Eddies detached from a jet crossing over a submarine ridge using a simple numerical model. (Submitted to J. Phys. Oceanogr.), 49 pp.

1. Introduction. This paper investigates the influences of a submarine ridge on a strong eastward jet using a two-layer quasi-geostrophic (QG) model on a  $\beta$  plane. Of particular interest is the influence of the ridge on the development of current meandering and eddies. The author notes possible application of the model results to the Kuroshio over the Shatsky Rise or the Emperor Seamount Chain, the Antarctic Circumpolar in the Drake passage, and the Gulf Stream over the New England Seamount Chain. Observations show that these currents exhibit behavior in the vicinity of the major topographic features that they don't exhibit elsewhere. Sometimes they are observed to split upstream of the ridge. There is also a tendency for cyclonic eddies to be generated on the western slope south of the eastward current and for anticyclonic eddies to occur on the eastern slope north of the current.

This paper presents some interesting and recent calculations, but does not nearly match the high caliber of the other papers summarized in this tech note. The author would greatly benefit from reading the literature, including some of the papers summarized here. Ikeda references only one theoretical paper other than his own, and does not give that a very meaningful reference.

2. Basic equations, ridge locations, initial and boundary conditions, and numerical method. The model equations are two-layer quasi-geostrophic potential vorticity equations in conservative form. The nondimensional parameters in the model equations are a depth ratio  $d = D/H = .3$ , an internal rotational Froude number  $F = f_0^2 L^2/g'H = 1$ , and a  $\beta$ -plane parameter (inverse beta Rossby number)  $b = \beta L^2/U = .1$ , where  $D$  is the upper layer thickness,  $H$  is the total depth,  $f_0$  is the reference value of the Coriolis parameter,  $L$  is the half-width of an initial zonal jet,  $g' = g\Delta\rho/\rho_0$  is the reduced gravitational acceleration,  $\beta$  is the variation of the Coriolis parameter with latitude and  $U$  is the maximum speed of the initial jet. Time is scaled by  $L/U$ . An internal Rossby radius of deformation is  $(d(1-d)/F)^{1/2} = .46$ . The amplitude of the Gaussian ridge is that of the Rossby number  $\epsilon = U/f_0 L$ .

The uniform N-S ridge is located near the center of the domain and has a half-width of 1.4. The zonal (longstream) extent of the domain is 27, the north-south extent is 14. The model is initialized with a zonal jet in the upper layer and a quiescent lower layer. The most unstable wave in a no ridge case had a wavelength of 4.5 which lead to eddies with a diameter ~ 1.8. A small amplitude perturbation with approximately this wavelength is superimposed on the initial jet west (upstream) of the ridge.

This paper discusses five numerical experiments, four of which involve successive quarter wave displacements between the ridge and the initial perturbation. The fifth has a flat bottom. The eastern and western boundaries are open. On the western (upstream) boundary, the x-derivatives of the pressure and potential vorticity are set to zero to avoid oblique streamlines on the boundary. On the eastern boundary the pressure and potential vorticity are fixed until  $t=30$ . After  $t=30$ , these quantities are assumed to propagate through the boundary at a prescribed speed of  $C_D = .15$ , since that is the time at which the first significant perturbation reaches the downstream boundary. The value of  $C_D$  was chosen to match the phase velocity in an earlier periodic solution (Ikeda, 1981). The author claims to have demonstrated that the open boundary conditions do not seriously deform the interior flow. Free slip is used for the northern and southern boundaries.

The reader is referred to Ikeda (1981) for details of the numerical model, a paper still in press at this writing. How dissipation of the enstrophy cascade is handled by the model is not entirely clear from the present paper. It is not done by explicit diffusion in the model equations. Apparently, it is handled by the use of highly numerical diffusive upstream differencing for advection and by applying a five-point smoother to the potential vorticity field at  $t=30$  and  $t=36$ . If so, this is an inferior approach to the dissipation problem in a numerical model.

3. Flow patterns. In the no ridge case all the meanders propagate eastward (downstream) and amplify. In general the smaller meanders tend to overtake the larger ones downstream, triggering the detachment of cyclonic eddies on the south side and anticyclonic eddies on the north side of the jet. Once the eddies detach, the amplitude of the meander is greatly reduced.

The ridge cases show no significant differences from the no ridge case until  $t \sim 18$ , since initially the lower layer is quiescent and time is required for it to receive sufficient energy from the upper layer to provide a back interaction influenced by the topography. Ikeda compares the results for ridge vs. no ridge solutions at greater times. (1) He finds that the ridge tends to promote the detachment of eddies, since the eddies are detached sooner and closer to the jet axis (i.e. from small amplitude meanders) in the presence of the ridge. (2) Detached cyclonic eddies are strengthened south of the jet on the western slope of the ridge, and anticyclonic eddies are strengthened north of the jet on the eastern slope. (3) The jet tends to meander northward (southward) around a high (low) on the western (eastern) slope of the ridge. (4) Detached eddies show a greater tendency to coalesce with the stream in the cases with the ridge. Ikeda suggests that this is due to f/h steering by topographic Rossby waves, with northward movement along the western slope and southward along the eastern. (5) In one case the jet split into two branches just upstream (west) of the ridge as a result of the coalescence. (6) The lower layer eddies have scales which are smaller when the ridge is present. In the flat-bottom experiment the lower layer eddies tend to become elongated zonally.

4. Method of examining topographic effects. To examine the influence of the topography on the relative vorticity, Ikeda vertically integrates the potential vorticity equations for each layer. He then (1) plots maps of the relative vorticity tendency due to topography, (2) integrates the layer integrated equations zonally and in time to investigate the potential vorticity budget as a function of latitude in order to estimate the importance of the topographic effect, and (3) studies the energy transfers among zonal Fourier components using Fourier transforms and an assumption of unperturbed flow of the zonal jet outside the model domain. Only transfers of total energy as a function of wavenumber due to topography and not due to topography are considered.

5. Mechanisms of bottom topographic effects. Based on the topographic contribution to the relative vorticity tendency, Ikeda anticipates anti-cyclonic (cyclonic) generation on the western (eastern) slope in the

presence of eastward flow over the ridge, and the opposite in the presence of westward flow. Ikeda claims to find this correspondence between flow in the lower layer and eddies in the upper layer. In some cases the vorticity budgets support the importance of the topography in generating specific eddies, but in some they do not.

Ikeda examines the jet splitting found in one of the cases upstream of the ridge by using the energy transfer spectrum analysis mentioned earlier. He finds that the topographic contribution is transferring energy from larger to smaller zonal wavenumbers at the time the splitting occurs, as required by the associated change in the flow pattern. At the time of the splitting the aggregate of transfers not due to topography does not show a transfer of energy to larger scales.

Finally, Ikeda notes that the flat-bottom experiment exhibits much larger zonally elongated gyres in the lower layer than do the experiments with a ridge. In all four ridge cases he finds that the topographic contribution transfers energy from low wavenumbers  $\lesssim .4$  to higher wavenumbers with a peak at  $\sim .6$ , in accord with the difference between the ridge and flat-bottom cases.

#### 6. Comparison with observations.

#### REFERENCE

- Ikeda, M., 1981: Meanders and detached eddies of a strong eastward-flowing jet using a two-layer quasi-geostrophic model. J. Phys. Oceanogr., 11, (in press).

## UNCLASSIFIED

SECURITY CLASSIFICATION OF THIS PAGE (When Data Entered)

REPORT DOCUMENTATION PAGE		READ INSTRUCTIONS BEFORE COMPLETING FORM
1. REPORT NUMBER NORDA Technical Note 109	2. GOVT ACCESSION NO. <i>AD-A103540</i>	3. RECIPIENT'S CATALOG NUMBER
4. TITLE (and Subtitle) A Summary of Papers Related to Mesoscale and Large-Scale Ocean Modeling		5. TYPE OF REPORT & PERIOD COVERED
		6. PERFORMING ORG. REPORT NUMBER
7. AUTHOR(s) Harley E. Hurlburt	8. CONTRACT OR GRANT NUMBER(s)	
9. PERFORMING ORGANIZATION NAME AND ADDRESS Naval Ocean Research & Development Activity Ocean Science & Technology Laboratory NSTL Station, Mississippi 39529		10. PROGRAM ELEMENT, PROJECT, TASK AREA & WORK UNIT NUMBERS
11. CONTROLLING OFFICE NAME AND ADDRESS Same		12. REPORT DATE June 1981
		13. NUMBER OF PAGES 93
14. MONITORING AGENCY NAME & ADDRESS (if different from Controlling Office)		15. SECURITY CLASS. (of this report) UNCLASSIFIED
		15a. DECLASSIFICATION/DOWNGRADING SCHEDULE
16. DISTRIBUTION STATEMENT (of this Report)  Unlimited		
17. DISTRIBUTION STATEMENT (of the abstract entered in Block 20, if different from Report)		
18. SUPPLEMENTARY NOTES		
19. KEY WORDS (Continue on reverse side if necessary and identify by block number) Mesoscale eddies                    Quasi-geostrophic Energetics Flow instabilities Ocean modeling Numerical simulations		
20. ABSTRACT (Continue on reverse side if necessary and identify by block number) This technical note contains summaries of the important ideas and results from 13 papers related to mesoscale and large-scale ocean modeling. Most of the papers represent major contributions to our understanding of the dynamics and energetics of mesoscale eddies and their interaction with ocean currents and with each other. Understanding the nature of flow instabilities associated with the generation and evolution of the eddies is an important aspect of the problem which receives much attention in these papers. Most of (CONTINUED)		

UNCLASSIFIED

SECURITY CLASSIFICATION OF THIS PAGE (When Data Entered)

the numerical simulations utilized simple two-layer, eddy-resolving, quasi-geostrophic models; a small number used primitive equation models.

E. M. S.

UNCLASSIFIED

SECURITY CLASSIFICATION OF THIS PAGE (When Data Entered)